Kristin Lode

Investigating the effects of inhibiting cytosolic phospholipase A2 alpha in an acute lymphoid leukaemia cell model

Master's thesis in Biotechnology
Supervisor: Berit Johansen
May 2019

Master's thesis

NTNU
Norwegian University of Science and Technology
Faculty of Natural Sciences
Department of Biology

NTNU
Kunnskap for en bedre verden

Kristin Lode

Investigating the effects of inhibiting cytosolic phospholipase A2 alpha in an acute lymphoid leukaemia cell model

Master's thesis in Biotechnology
Supervisor: Berit Johansen
May 2019

Norwegian University of Science and Technology
Faculty of Natural Sciences
Department of Biology

NTNU
Norwegian University of
Science and Technology

Til Andrea og Heidrun

Acknowledgement

In this Master of Science, the role of cPLA$_2\alpha$ in the acute lymphoid leukaemia cell line CCRF-CEM has been investigated. The thesis is the result of the five year master program of Biotechnology at NTNU, Trondheim. The thesis was carried out from the fall of 2017 to the spring of 2019 under the supervision of Prof. Berit Johansen via Avexxin AS and NTNU. I would like to thank her for her guidance and inspiration throughout this project.

Trondheim, May 15th 2019
Kristin Lode

Forord

Arbeidet med denne masteroppgaven de siste to årene har vært et sant eventyr. Jeg har fått en forsmak på hva forskning virkelig er med alt det innebærer. Jeg har både fått erfare den enorme gleden i forbindelse med gode resultat, men også frustrasjonen ved nok et feilslått forsøk. Samlet sett har jeg hatt to fantastiske år, og i den forbindelse er det flere som fortjener en takk.

Først og fremst ønsker jeg å takke hovedveilederen min, Berit Johansen, for hennes veiledning og smittende entusiasme for $cPLA_2$. Takk til alle mine tre biveiledere; Linn-Karina Selvik, Thuy Nguyen og Astrid Jullumstrø Feuerherm for lærerike diskusjoner, oppmuntrende ord og evaluering av arbeidet mitt de siste to årene. Jeg ønsker også å takke resten av $cPLA_2$-gruppen ved Avexxin AS; Felicity, Anfal, Nur og Elisabeth for deres hjelp, samarbeid og trivelige samtaler.

En spesiell takk må også rettes til Kristin Grendstad som tok seg tid til å hjelpe meg med flowcytometri, og ikke minst for å ha åpnet øynene mine for hvor morsomt flowcytometri er. Det har vært en glede å jobbe med deg!

Vennene mine har selvfølgelig også betydd utrolig mye. Takk til Torill for uttallige lange lunsjpauser gjennom fem år og for alle motivasjonstaler den siste tiden. En stor takk må også rettes til min gode venn Kristin som alltid stiller opp.

Til slutt vil jeg takke verdens beste heiagjeng, min fantastiske familie. Takk til mamma og pappa for deres endeløse støtte, oppmuntring og kjærlighet. Takk til mine fantastiske søstre og beste venner, Andrea og Heidrun, jeg hadde ikke klart dette uten dere. Andrea, jeg setter uendelig stor pris på ditt upåklagelige engasjement i denne graden, for dine mange råd om hvordan jeg kan takle utfordringene som oppstår i et masterløp, og ikke minst for at du har vært tidenes beste rubber duck og for at du alltid tror på meg. Heidrun, jeg setter umåtelig stor pris på at du alltid etter beste evne svarte på mine mange spørsmål, for all tiden du har brukt på korrekturlesing og fremfor alt for at du har inspirert meg til å følge forskerdrømmen.

Abstract

Leukaemia is the most common childhood cancer and approximately 80% of these incidences are categorised as acute lymphoid leukaemia (ALL). ALL represents a heterogeneous group of diseases without an identifiable genetic or environmental cause, and therefore lacks targeted treatment. To develop better treatments for this subtype of leukaemia, the molecular mechanisms at play must be unravelled.

To address this very important issue, we investigated cytosolic phospholipase $A_2\alpha$ ($cPLA_2\alpha$) as a novel therapeutic target in T-ALL. Four $cPLA_2\alpha$ inhibitors (Compounds 1-4 developed by Avexxin) specifically targeting the phospholipase activity of the enzyme and one phosphoinositide 3-kinase inhibitor (Buparlisib/BKM120) were studied in the patient derived cell line CCRF-CEM. All the agents, except Compound 3, reduced viability in a dose dependent manner. Combinations of suboptimal doses of Compounds 1 and 2 with BKM120 were found to act in synergy according to combination indexes calculated by Bliss Independence. Interestingly, cell death assays suggested that mode of death after treatment with $cPLA_2\alpha$ inhibitors and BKM120 were dependent on the serum concentration, regardless of the inhibitors. The inability of the $cPLA_2\alpha$ inhibitors to induce cell cycle arrest is in line with the current notion that $cPLA_2\alpha$ promote cell cycle arrest independently of its phospholipase activity.

By inspecting the $cPLA_2\alpha$ contribution on cell viability and cell cycle progression in this T-ALL model system, $cPLA_2\alpha$ was proven to be a promising therapeutic target. Several inhibitors from Avexxin could serve as both chemopreventive single agents or in combination with established treatments in the future. Additionally, the inhibitors showed potential as potent therapeutics in personalised medicine for T-ALL and other cancer types displaying deregulation of $cPLA_2\alpha$. Our data will pave the way for further studies addressing how treatment can be targeted more directly toward essential signalling pathways disrupting cancer progression.

Sammendrag

Leukemi er den vanligste kreftformen blant barn, og tilnærmet 80% av alle tilfellene kategoriseres som akutt lymfatisk leukemi (ALL). ALL representerer en heterogen gruppe av sykdommer uten et identifiserbart genetisk eller miljøbasert opphav, og mangler derfor målrettet behandling. For å utvikle bedre medisiner i behandling av denne omfattende undergruppen av leukemi, er det avgjørende at de underliggende molekylære mekanismene kartlegges.

For å rette oppmerksomhet mot denne viktige problemstillingen har vi undersøkt cytosolisk fosfolipase $A_2\alpha$ ($cPLA_2\alpha$) som et nytt terapeutisk mål i T-ALL. Fire $cPLA_2\alpha$ inhibitorer (Compounds 1-4 utviklet av Avexxin) som spesifikt inhiberer enzymets fosfolipaseaktivitet, samt én fosfoinositid 3-kinase inhibitor (Buparlisib/ BKM120) ble studert i den pasientderiverte cellelinjen CCRF-CEM. Alle inhibitorene, med unntak av Compound 3, reduserte celleviabiliteten på en doseavhengig måte. Da suboptimale doser av Compound 1 og 3 ble gitt i kombinasjon med suboptimale doser av BKM120, viste det seg at de virker i synergi i følge kombinasjonsindekser beregnet med Bliss Indepedence. Assay som ble gjennomført for å granske celledød etter behandling med inhibitorene antydet at induksjon av apoptose og nekrose var avhengig av serumkonsentrasjonen i mediet. Den manglende evnen til å indusere cellesyklusarrest for $cPLA_2\alpha$ samsvarer med nåværende teori om at $cPLA_2\alpha$ fremmer cellesyklusarrest uavhengig av sin fosfolipaseaktivitet.

Ved å undersøke bidraget til $cPLA_2\alpha$ i dette modellsystemet for T-ALL, ble $cPLA_2\alpha$ vist å være et lovende terapeutisk mål. Flere inhibitorer fra Avexxin kan i fremtiden både fungere kjemopreventivt som enkeltkomponenter eller i kombinasjon med etablerte behandlinger. I tillegg viste inhibitorene potensiale som potente terapier i personrettet medisin i T-ALL og andre krefttyper med feilregulering av $cPLA_2\alpha$. Våre data vil kunne bane vei for videre studier som adresserer hvordan behandling spesifikt kan rettes mot essensielle signalveier som regulerer kreftutvikling.

Abbreviations

AA	Arachidonic acid
ACD	Accidental cell death
ALL	Acute lymphoid leukaemia
AML	Acute myeloid leukaemia
BKM120	Buparlisib
BM	Bone marrow
BP	Bandpass
CGM	Complete growth medium
CI	Combination index
CLL	Chronic lymphoid leukaemia
CML	Chronic myeloid leukaemia
COX	Cyclooxygenase enzyme
$cPLA_2$	Cytosolic phospholipase A2
$cPLA_2\alpha$	Cytosolic phospholipase A2 alpha
DMSO	Dimethyl sulfoxide
FBS	Foetal bovine serum
FS	Forward scatter
G_1 phase	G1 phase of the cell cycle

G_2 phase	G2 phase of the cell cycle
HETE	Hydroxyeicosatetraenoic acid
HSC	Haematopoietic stem cell
IC50	Half maximum inhibitory effect
IKK	I kappa B kinase
LOX	Lipoxygenase enzyme
LT	Leukotriene
LTA_4	Leukotriene A_4 hydrolase
LTB_4	Leukotriene B_4
LX	Lipoxin
M phase	Mitotic phase of the cell cycle
MRD	Minimal residual disease
NF-$\varkappa$B	Nuclear factor kappa B
PAF	Platelet activating factor
PDT	Population doubling time
PG	Prostaglandin
PGE_2	Prostaglandin E_2
PI	Propidium iodide
PI3K	Phosphoinositide 3-kinase
PIP_2	Phosphatidylinositol 4,5-bisphosphate

PLA_2	Phospholipase A_2
RCD	Regulated cell death
RFU	Relative fluorescent unit
rpm	Revolutions per minute
RT	Room temperature
S phase	Synthesis phase of the cell cycle
SCT	Stem cell transplantation
SM	Starvation medium
TNF	Tumour necrosis factor
TOF	Time of flight
TX	Thromboxane

Table of contents

1 Introduction

In this section, fundamental concepts of this thesis is introduced. Due to the scope of the different experiments, theory underlying each experiment is provided in section 3 Materials and methods.

1.1 Cancer

In the Oxford Dictionary, cancer is defined as *"a disease caused by an uncontrolled division of abnormal cells in a part of the body"* [1]. This comprehensive definition reflects the numerous factors that contribute to the development and occurrence of cancer. Such factors include, but are not limited to; viral infections, chronic inflammation, diet and age [2]. Regardless of the cancer causative mechanism, all these risk factors exert their effects on one of two classes of genes; tumour suppressor genes and proto-oncogenes [3, 4].

Tumour suppressor genes are involved in the regulation of cell division, DNA repair mechanisms and susceptibility of apoptosis [5]. These functions are of vital importance to the organism as they prevent cells with mutated genomes to divide and survive. Mutations in tumour suppressor genes result in truncated and dysfunctional proteins, and can therefore be categorised as loss-of-function mutations [4, 5]. If the DNA cannot be repaired, apoptosis is induced and the potentially dangerous cell is eliminated [6]. In contrast, proto-oncogenes are drivers of cell proliferation and differentiation [7]. Mutations in these genes result in a gain-of-function of the translated protein, and the now cancer causing genes are termed oncogenes [3, 4]. Oncogenes promote cancer by allowing uncontrollable cell proliferation resulting in an accumulation of mutations, ultimately leading to the development of a cancer cell [3].

The development of cancer, carcinogenesis, is similar to natural selection and evolution [9]. This process can be divided into three distinct stages; initiation, progression and metastasis (Figure 1.1) [8, 10]. The initiation

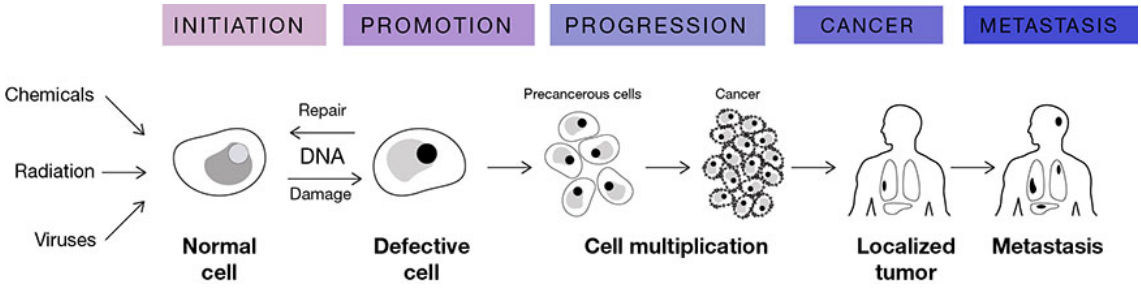

Figure 1.1: A schematic representation of the development of cancer. The cells accumulate mutations in the progression stage, allowing the tumour to adapt to its environment. Once the tumour become malignant and able to invade the surrounding tissue, it is referred to as cancer. The last stage of a cancer is metastasis, in which it spreads throughout the body [8]. Figure from Roomi *et al.* [8].

process is triggered by the original stimuli or mutation that induce DNA damage, allowing the cell to proliferate uncontrollably [9]. Additional mutations follow the abnormal proliferation in the progression stage, and the fastest growing cells are subjected to positive selection [11]. The cellular population may consist of several genetically different subclones, giving rise to a heterogeneous tumour [9, 12]. To sustain its own growth, the tumour secretes an array of proteins, including growth factors. In addition to stimulate and allow the tumour cells to grow, growth factors also promote the formation of new blood vessels through the process of angiogenesis. With the increased blood supply, the tumour attains sufficient access to oxygen and nutrition to support its accelerated expansion. Once the tumour is able to invade the surrounding tissue, it is referred to as malignant. Only malignant tumours are recognised as true cancers [11]. Metastasis, the last stage, is the most dangerous and least understood mechanism of cancer. To colonise tissues at distant sites, the cancer cells must invade the surrounding tissue, enter the circulatory system, leave the vessels and establish a new cellular colony at a distant site. With time, this new colony evolve into a metastatic tumour [9, 11].

1.2 Leukaemia

Leukaemias account for approximately 8% of all human malignancies and arise from haematopoietic stem cells (HSC) [11, 13]. As HSCs differentiate

and commit to either the myeloid or lymphoid lineage (Figure 1.2), the cells gradually lose their potential of both differentiation and self renewal [14]. Leukaemic cells fail to go through terminal differentiation, and become arrested at earlier stages of maturation. In this state, the cells maintain their ability to proliferate, resulting in an accumulation of immature cells [11, 15]. Differentiation therapy in which the immature cells are forced to differentiate and mature is associated with reduced leukaemic cell mass and clinical remission [15]. The arrested differentiation can thus be considered causative of leukaemia.

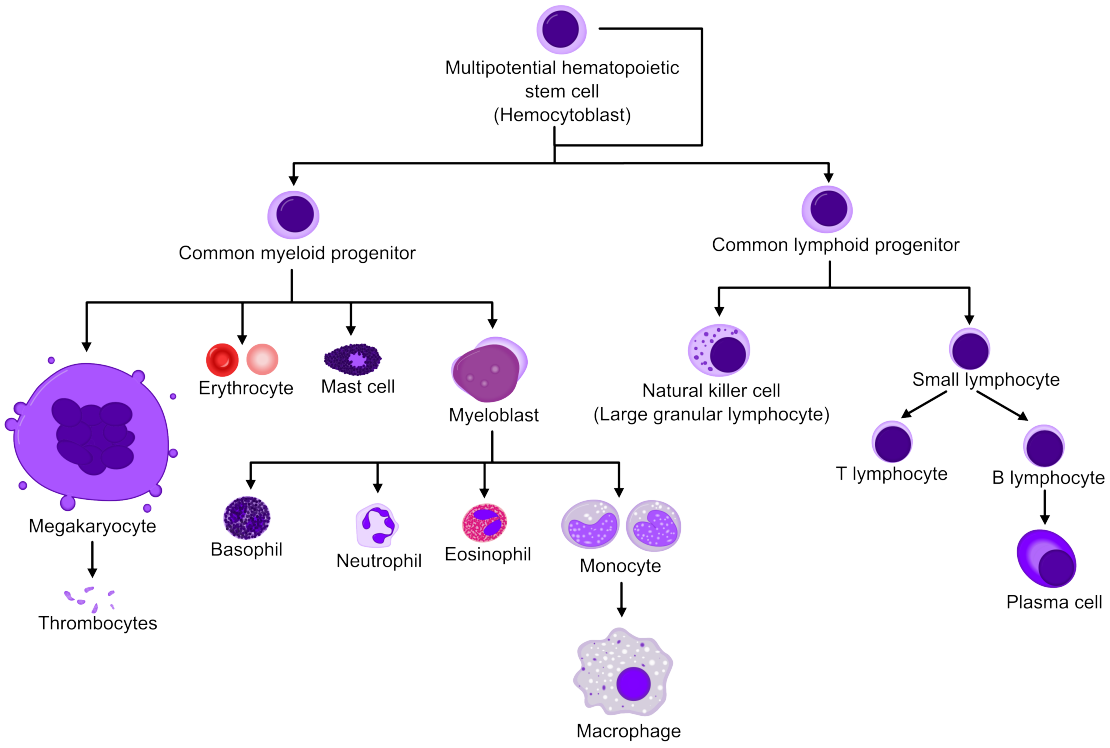

Figure 1.2: All the cellular elements of the blood, from red blood cells that transport oxygen to immune cells, ultimately derive from the haematopoietic stem cells (HSC) of the bone marrow. As the HSC divides, they can produce one of two types of stem cells, the common myeloid progenitor and the common lymphoid progenitor which in turn give rise to the myeloid and lymphoid cell lineages, respectively [16]. Most of the immune cells mature in the bone marrow before travelling through the blood to peripheral organs. Some cells undergo further maturation outside the bone marrow, such as T lymphocytes which develop into maturity in the thymus [17]. Figure from Häggström & Rad with permission [18].

Human leukaemia can be divided into four subgroups based on the cell lineage and clinical manifestation (Figure 1.3). Acute leukaemia display an

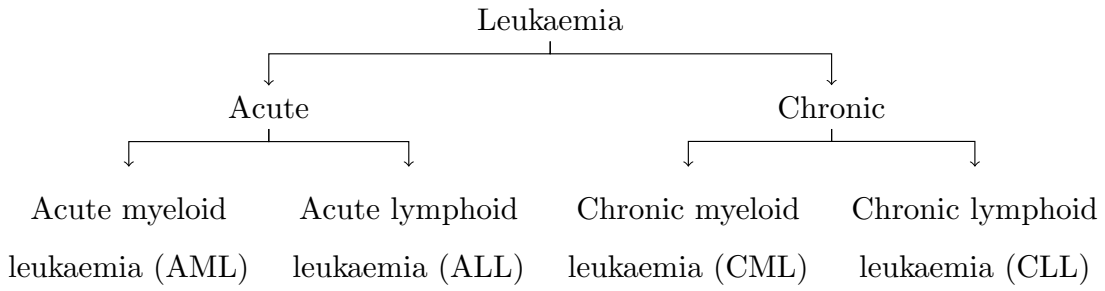

Figure 1.3: A schematic representation of the classification of leukaemia.

abrupt manifestation and disease onset, whereas chronic leukaemia display a slow manifestation [19]. Acute leukaemias are associated with aggressive and usually fatal diseases, unless treated immediately [20]. Both acute myeloid leukaemia (AML) and acute lymphoid leukaemia (ALL) are most prevalent amongst young children. Due to their slow onset, chronic myeloid leukaemia (CML) and chronic lymphoid leukaemia (CLL), are most commonly found in the older population [21].

1.3 Acute lymphoid leukaemia

Acute lymphoid leukaemia (ALL) represent 12% of all leukaemia cases, and approximately 80% of all leukaemia cases amongst children [22]. The heterogeneous group of diseases have two prevalence peaks; one at the ages between 2 and 5 years, and the second after the age of 50 [23, 24]. The majority of ALL patients do not display an identifiable genetic or environmental cause. Genetic mutations, hereditary links and exposure to carcinogenic factors are however believed to be the most prominent risk factors [22]. This is also evident by the nature of the genetic mutations identified in ALL which cause uncontrollable proliferation, as well as prevent normal differentiation [22]. As a result, early haematopoietic cells, called blast cells, accumulate in the bone marrow [23]. Clinical manifestations of ALL are characterised by anaemia and leucopenia as the bone marrow fails to exert its normal function. Secondary symptoms include fever, weight loss, easy bleeding or bruising and infections [25].

1.3.1 Treatment of acute lymphoid leukaemia

The diagnosis of ALL is based on the presence of 20% or more lymphoblasts in the bone marrow or peripheral blood circulation. Morphology, immunophenotype and cytogenetics are used to both confirm the diagnosis, and to assess risk stratification. An accurate risk stratification is important to determine an appropriate initial treatment [25].

Current treatment of ALL is mainly consisting of chemotherapy, which in some cases is followed by stem cell transplantation (SCT) [25]. The survival rate amongst paediatric ALL is approaching 90%, whereas adults with ALL display an overall survival rate of 50 - 70% [25, 26]. The initial response to treatment is indicative of the overall outcome for the patient. Previously, the response was evaluated based on morphology of cells, while recent advances allow for more elaborate and accurate evaluation of the patients' minimal residual disease (MRD) using flow cytometry and PCR [25]. MRD is essentially the detection of residual leukaemic cells, which are not detectable by light microscopy [27]. When present in patients after initial treatment, MRD is used to adapt future treatment, usually consisting of an intensification of chemotherapy amongst paediatric patients, and SCT in adults [25, 28].

1.3.2 The CCRF cell line

Foley *et al.* created a continuous cell line of human T lymphoblasts from peripheral blood of a child with acute leukaemia in 1965 [29]. The female child, C. E. M. aged three, was diagnosed with acute lymphoid leukaemia in 1963. Four samples of peripheral blood were drawn for cell culture in 1964, in which one was used to establish the CCRF-CEM (ATCC® CLL-19™) cell line, and the remaining samples were used for biochemical and biological studies [29]. CCRF-CEM cells are grown in suspension, and therefore display a more homogeneous morphology compared to other adherent cell line models for T-ALL [30].

1.4 The cell cycle

Human cells in culture divide approximately once every 24 hours. When viewed in the microscope, the cell cycle can be distinguished into two parts; interphase in which the cell is growing, and the nuclear division in mitosis. However, at a molecular level, the cell cycle can be distinguished into four phases based on the timing of DNA synthesis (Figure 1.4) [31].

The mitotic (M) phase of the cell cycle consist of both the nuclear division (mitosis), and the division of cytoplasm (cytokinesis) [31, 32]. Despite being the shortest phase of the cell cycle, only lasting for about an hour, it is the most dramatic for the cell [31]. Errors during the separation of chromosomes might result in non-viable cells, and the mechanisms involved in these processes are therefore tightly regulated [32].

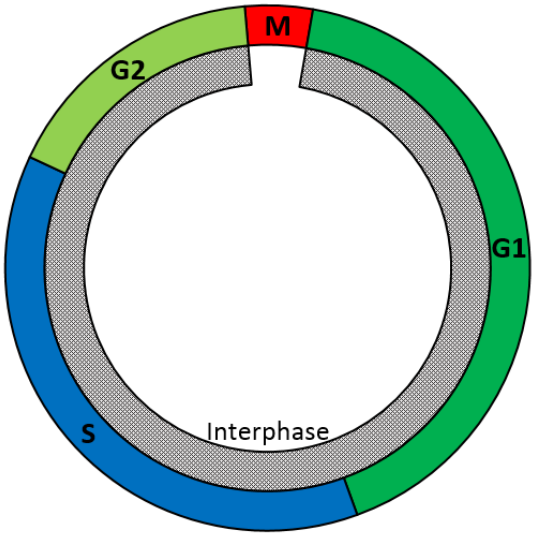

Figure 1.4: The eukaryotic cell cycle can be divided into four distinct phases; mitosis, G_1, S and G_2. The cell grows throughout interphase, which includes G1, S and G2, indicated in the grey shaded area. The relative lengths of the phases of the cell cycle are typical for that of a rapidly replicating mammalian cell. Adapted from Cooper [31].

The M phase is followed by gap phase 1 (G_1). This phase is defined as the interval between mitosis and the initiation of DNA synthesis for replication. During this phase, the cell is metabolically active and grows continuously [31]. In addition to grow, the cell also monitor both its internal and external environment to ensure that it is suitable to progress into synthesis (S) phase and eventually mitosis in M phase. If the conditions are deemed unsuitable, the cell may enter a specialised resting state termed G_0, in which it can remain for a prolonged period of time before it resumes proliferation [32]. Once in the S phase, the cell begins to replicate its DNA in preparation of cell division. As a consequence, the DNA content in the cell doubles from normal 2n to 4n. The cell will have a

4n DNA content until cytokinesis after mitosis [31]. After DNA replication, the cell enters G_2, in which it continues to grow and synthesise the necessary proteins for mitosis [31]. Before transitioning to M phase, control mechanisms ensure that all the DNA is replicated, and that the cell environment still is suitable for cell division [32]. Unless any problems are detected, the cell enters M phase, and its DNA content is again reduced to 2n [31].

1.5 Mechanisms of cell death

Cell death is just as important as the progression through the cell cycle and proliferation. The Nomenclature Committee on Cell Death has defined 12 different major subroutes for regulated cell death (RCD) based on mechanistic and essential aspects of the processes. In contrast to accidental cell death (ACD) induced by chemical, physical or mechanical conditions, RCD depends on a dedicated molecular machinery. This suggests that pharmacological or genetic intervention may modulate the process, either by delaying or accelerating RCD [33].

When observing dying cells under the microscope, three different morphotypes can be distinguished; i) apoptosis in which the cell displays a shrinkage of the cytoplasm, condensation of chromatin, fragmentation of the nucleus and blebbing of the plasma membrane, ii) autophagy where the cytoplasm is extensively vacuolised, followed by phagocytic uptake and lysosomal degradation and iii) necrosis in which the cell does not display any features as in i) and ii) and the cell corps is disposed of in the absence of phagocytic and lysosomal involvement [33].

Apoptosis is an important homeostatic mechanism to balance the effects of mitosis in the regulation of cell number in multicellular organisms. In addition to its regulatory functions, apoptosis also has a protective function as it is used to remove transformed, infected and injured cells which may be harmful for the organism. Key characteristic traits of apoptosis include shrinkage of the cell, nuclear condensation, blebbing of the plasma membrane, DNA fragmentation and externalisation of phosphatidylserine [35].

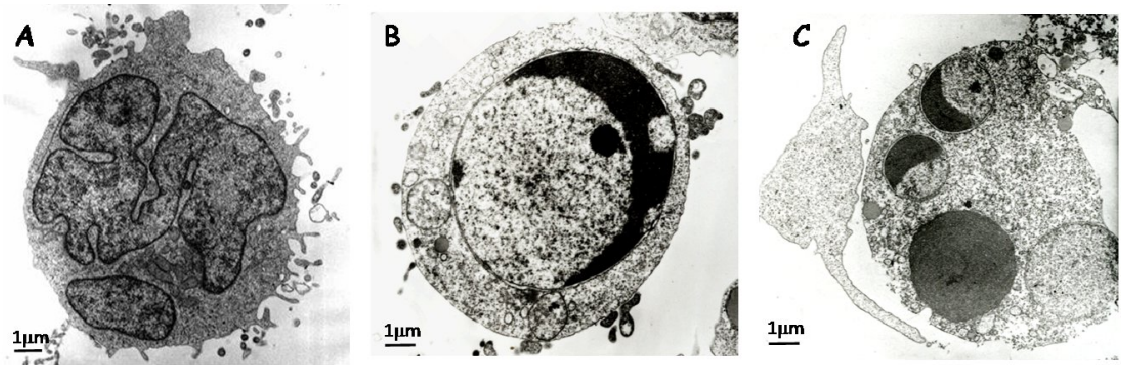

Figure 1.5: Electromicrograph of CCRF-CEM cell undergoing apoptosis. Normal cell seen in (A), characterised with its large nucleus and lack of obvious vacuoles. Cells undergoing apoptosis (B-C) display increased vacuolisation of the cytoplasm, marginalisation of condensed chromatin (B) and formation of micronuclei (C). Figure from Apraiz *et al.* with permission [34]

Several of these changes can be visualised under the microscope (Figure 1.5) [34]. The process of apoptosis is regulated, and can either be induced in cells by activating extracellular signals, or by the lack of signals required for survival [36]. Once induced, apoptosis is under the strict molecular control coordinated by a set of cysteine proteases termed caspases and their regulators [35].

In contrast to the strictly regulated process of apoptosis, cell death through necrosis is characterised by rapid rupture of the cell membrane, followed by subsequent release of endogenous danger signals. The release of these factors induce local inflammation, and is thus a more dramatic mode of death compared to apoptosis [35].

1.6 Arachidonic acid and cytosolic phospholipase A_2

Cancer is considered a disease of ageing as the average cancer patient is over the age of 55 [37]. This is partly due to the exponential accumulation of potentially dangerous somatic mutations in tumour suppressor genes and proto-oncogenes with increasing age [38]. A second mechanism at play is immune senescence, a form of degeneration of the immune system that occurs with age. In addition to render the individual less protected against

pathogens, it also results in overactive inflammatory mechanisms. In this meta-inflammatory state, there is an increased production and secretion of growth factors and angiogenic factors. When combined, such factors make the ideal microenvironment for tumour growth [37].

Upon inflammatory stimuli or stress, cells produce intracellular lipid mediators to confer and maintain the inflammatory signal [39, 40]. Phospholipase A_2 (PLA_2) belongs to a superfamily of enzymes responsible for hydrolysing the *sn-2* fatty acids of membrane phospholipids to form arachidonic acid (AA) [40, 41]. The superfamily of enzymes include 15 groups comprising four main types, namely the secreted, cytosolic, calcium independent cytosolic and platelet activating factor (PAF) acetyl hydrolase/oxidised lipid lipoprotein associated PLA_2 [42, 43]. The subgroup of calcium dependent cytosolic PLA_2 ($cPLA_2$) is the only PLA_2 with a preference for AA in the *sn-2* position of phospholipids [42].

Since its identification in human platelets in 1986, six paralogues of $cPLA_2$ have been identified, namely $cPLA_2\alpha$ - ζ, all of different molecular weight. $cPLA_2\alpha$ (Figure 1.6), a 85 kDa protein, consists of two distinct domains; a calcium binding domain (C2) and a catalytic α/β hydrolase domain [40, 44]. The C2 domain is located at the N-terminal end of the protein, and is used to dock the protein to the plasma membrane [40]. This binding is mediated by three mechanisms; i) Ca^{2+} mediated translocation, ii) binding of secondary lipid messengers and iii) phosphorylation [42]. When Ca^{2+} associates with the C2 domain, the protein binds to the lipid surface of the plasma membrane by penetration of Ca^{2+} binding loops into the interface of the membrane [42]. Once bound to the membrane, the enzyme interacts with phospholipid molecules that induce a conformational change of the enzyme, exposing its active site in the C-terminal β-barrel catalytic unit [40, 42, 45]. This conformational change include the opening of the lid region spanning the active site [44]. In its normal state, the lid region covers the active site and prevents substrates from binding to the active site before the enzyme receives activating signals [42, 45]. One such activating signal is the phosphorylation of Ser505, believed to cause a conformational

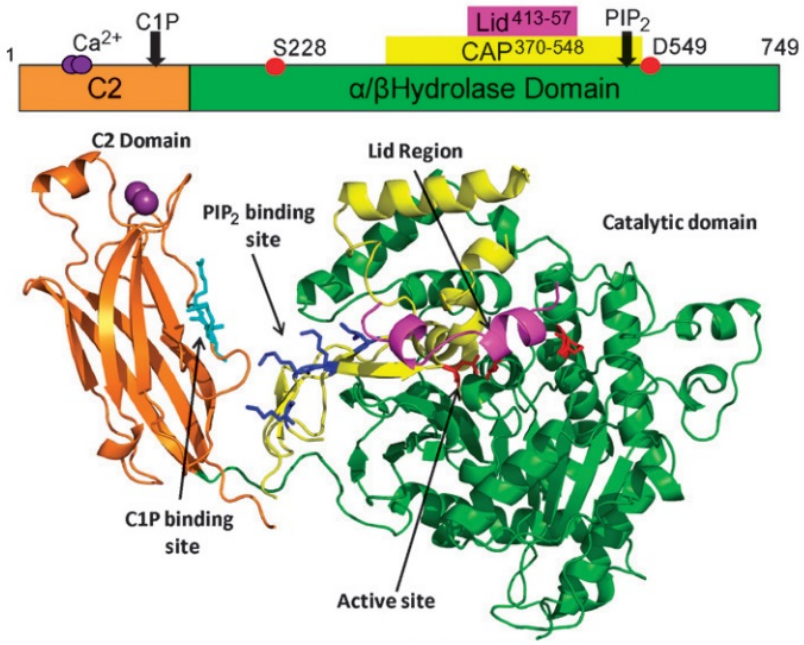

Figure 1.6: The crystal structure of cPLA$_2\alpha$ determined by Dessen *et al.* [46]. The C2 domain is shown in orange, with two Ca^{2+} ions shown in purple. The catalytic domain is shown on the right hand side, with the lid region coloured magenta. The active site is shown in red. Figure from Burke & Dennis with permission [44].

change of the active site, improving its binding ability to the substrate [45]. cPLA$_2\alpha$ can also be activated by phosphatidylinositol 4,5-bisphosphate (PIP_2) independently of Ca^{2+}. When PIP_2 is bound to its binding site in the catalytic domain, the enzyme display an increased catalytic efficiency [42].

Free AA can be metabolised along three different pathways to become oxygenated bioactive signalling molecules termed eicosanoids (Figure 1.7) [45]. When metabolised along the cyclooxygenase (COX) pathway, enzymes COX-1 and COX-2, along with terminal synthases, produce prostaglandins (PG) and thromboxane (TX). These biomolecules exert their function through a series of G-protein coupled receptors [45]. Alternatively, free AA can be metabolised along the lipoxygenase (LOX) pathway by central enzymes 5, 12 and 15-lipoxygenase (5-LO, 12-LO and 15-LO) and leukotriene A_4 hydrolase (LTA_4) to produce several classes of leukotrienes (LT) and lipoxins (LX) [45]. When metabolised along the P-450 epoxygenase pathway, also

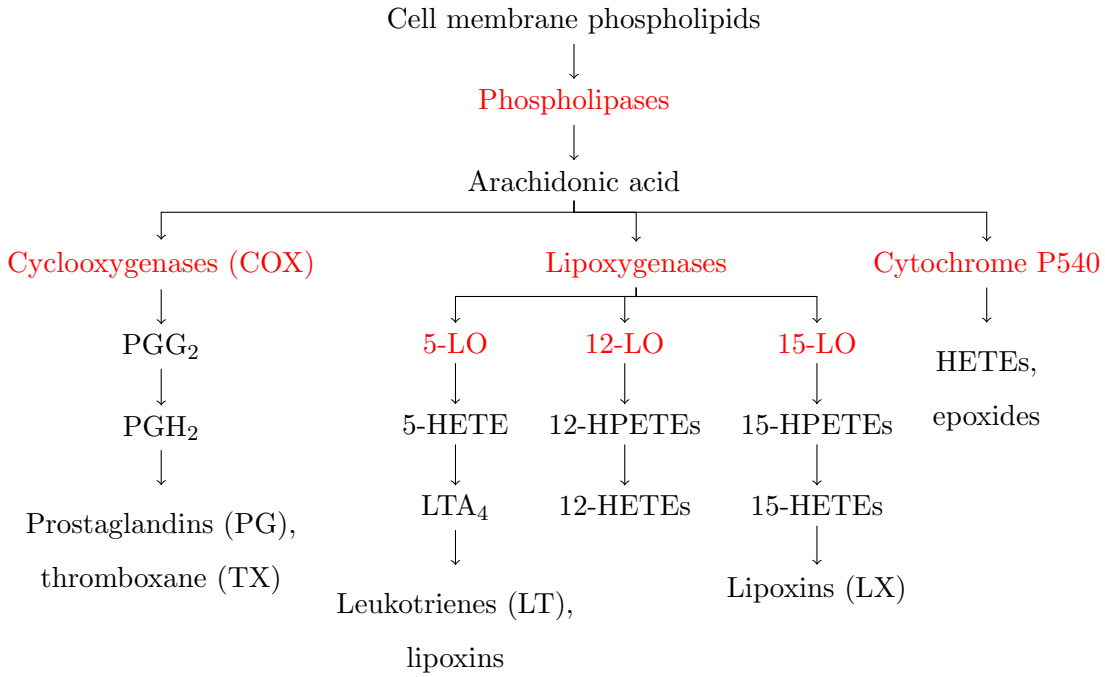

Figure 1.7: A simplified schematic representation of the eicosanoid pathway. Phospholipids with fatty acids in the *sn-2* position of the plasma membrane are hydrolysed by cPLA$_2\alpha$ to form arachidonic acid (AA). Free AA may be metabolised in the cyclooxygenase (COX) pathway to generate prostaglandins and thromboxane, along the lipoxygenase (LOX) pathway to produce leukotrienes and lipoxins, or along the P450 epoxygenase pathway to produce hydroxyeicosatetraenoic acids (HETEs) and epoxides. The various eicosanoids have different physiological effects [45, 47]. Enzymes are presented in red. Adapted from Harizi *et al.* [47].

called cytochrome P450, free AA is oxidised to hydroxyeicosatetraenoic acids (HETEs) and epoxides [47].

AA derived eicosanoids are involved in the complex regulation of various aspects of the immune system, such as the production of cytokines and formation of antibodies, in addition to central physiological processes like cell migration, proliferation and differentiation [47].

2 Rationale for the study

Already in 1863, the Polish doctor Rudolf Virchow postulated that cancer cells originated from inflammatory sites in the body [48, 49]. Advances in mapping of the tumour microenvironment the last two decades have supported Virchow's hypothesis [48, 50]. Today, the interaction between inflammation and cancer is widely accepted [50]. Current research is attempting to unravel the molecular links between inflammation and cancer, aiming to develop anti-inflammatory therapeutics for the prevention and treatment of cancer [49, 51]. One such link is the eicosanoids which are known to be lipid mediators of inflammation, and have also been found implicated in several cancers [52, 53]. As the principal producer of eicosanoids, cPLA$_2\alpha$ is presenting itself as a great potential therapeutic target in cancer.

The pharmaceutical company Avexxin has developed an array of inhibitors specific for cPLA$_2\alpha$. These inhibitors inactivate the enzyme's phospholipase activity through reversible competitive binding of the active site (Personal communication with Prof. Berit Johansen, Trondheim 22.03.2019). Previous studies have demonstrated the inhibitors' efficacy in breast cancer cell lines (unpublished results), and we wanted to further investigate the effect of inhibiting cytosolic phospholipase A$_2\alpha$ in the human acute lymphoid leukaemia cell line CCRF-CEM. To address this highly important task, the following aims were set for this thesis:

- Establishing the CCRF-CEM cell line as a model system through the characterisation of growth pattern and morphological traits
- Establishing dose response curves for selected cPLA$_2\alpha$ inhibitors and the PI3K inhibitor BKM120
- Investigating possible synergy between cPLA$_2\alpha$ inhibitors and BKM120
- Identifying mode of death following treatment with cPLAα inhibitors and BKM120
- Investigating the effect of cPLA$_2\alpha$ inhibitors and BKM120 on cell cycle progression

3 Materials and methods

3.1 Cell culture

CCRF-CEM (ATCC CCL-119) cells were grown according to the recommendations of the supplier [54]. The culture medium, RPMI-1640, was supplemented with 10 µL/mL glutamine, 2 µL/mL gentamicin and 10% foetal bovine serum (FBS) to make complete growth medium (CGM). The cells were incubated at 37°C in a humidified atmosphere with 5% CO_2. Passaging was conducted every 2 - 4 days to maintain a cell density below 2.5×10^6 cells/mL, and thus ensure a continuous proliferation. Cells were allowed to acclimatise for two weeks after establishment before they were utilised for experimental purposes and discarded after 25 passages. Information about reagents and general equipment used for cell cultivation and the following experiments can be viewed in Table A.2 in Appendix A.

3.2 Growth curve

To assert the time interval in which the cells were in an exponential growth phase, the development in cell density and viability were measured over a period of 7 days without changing the medium. The initial densities were 2.5×10^4 cells/mL, 1.0×10^5 cells/mL and 4.0×10^5 cells/mL. The cells were subcultured at their respective densities in a T75 flask, and both density and viability were measured in an automatic cell counter using trypan blue every 24 hours. The experiment was repeated three times, with three biological replicates. Population doubling time (PDT) during the exponential growth phase was calculated using

$$t_{\mathrm{d}} = \frac{t}{log_2(N_1/N_0)} \tag{1}$$

where t_{d} is the time required for doubling, t denotes the duration of the exponential growth phase, and N_0 and N_1 represent the cell density at the

beginning and end of the exponential growth phase, respectively [55].

3.3 Viability assay

Cell viability was measured using the non toxic redox dye resazurin. Upon reduction by mitochondrial enzymes in living cells, the dye is converted to a pink fluorescent dye, resorufin. The fluorescence emitted by resorufin upon excitation can be read using a microplate fluorometer or a spectrophotometer, where emitted fluorescence is directly proportional to the number of living cells [56]. Preliminary experiments allowed optimisation of cell density and incubation time with resazurin for cells in medium supplemented with 10% FBS (Appendix B).

To identify the half maximum inhibitory effect (IC50), the concentration in which 50% of the cells are dead, dose response relationships were investigated with increasing concentrations of inhibitors.

Cell cultures were seeded at 4.0×10^5 cells/mL 72 hours prior to the experiments to ensure that the cells were actively proliferating. Cells were seeded in 96 well plates at 5×10^4 cells/well in 80 µL in either CGM or in starvation medium (SM) supplemented with 0.5% FBS. The outermost wells were filled with medium instead of cells to avoid possible edge effects. The cells were incubated for 1 hour to allow them to settle prior to treatment with inhibitors. Working stocks of the inhibitors were made by diluting the inhibitors in dimethyl sulfoxide (DMSO). The final concentration of inhibitors were made by addition of SM. The concentration of DMSO in the treatments and control was standardised to 0.2%.

The cells were treated with inhibitors for 24, 48 and 72 hours before the viability was measured using resazurin. The plates were incubated with resazurin for 2 hours according to the manufacturer's protocol, before the plates were read at 544 nm excitation and 590 nm emission [57]. The experiments were repeated three times with cultures of different passage numbers. The dose response relationships were presented graphically using a variable

slope with four parameters. The curves were constructed using

$$y = P_{\mathrm{b}} + \frac{\Delta P}{1 + (x^S / IC50^S)} \tag{2}$$

in which P_b represent the bottom plateau, ΔP is the difference between the top and bottom plateau, S is the hill slope, IC50 is the half maximum and x is the treatment doses given in micro molar.

3.3.1 Combination assay

Combination of drugs as a therapeutic strategy against cancer has been studied since the 1960's [58]. Combining drugs with different sites of action may reduce adverse toxicities observed in the respective monotherapies and reduce drug resistance, whilst maintaining or improving the efficacy of the monotherapies [58–60]. Furthermore, combination therapies aim to achieve a synergistic drug effect. Synergy is defined as the greater effect of drugs in combination, compared to their additive effect as monotherapies [60]. There are several ways to classify the effect of a combination treatment as antagonistic, synergistic or additive [60]. Here, Bliss Independence was used to calculate a combination index (CI) for the investigated combinations. The CI was calculated using

$$CI = \frac{E_{\mathrm{A}} + E_{\mathrm{B}} - (E_{\mathrm{A}} \times E_{\mathrm{B}})}{E_{\mathrm{AB}}} \tag{3}$$

where E_A and E_B represent the effects of drugs A and B given as monotherapies, respectively, and E_{AB} represent drugs A and B given in combination at the same concentrations as the monotherapies. A CI of less than 1 indicate synergy and a CI of more than 1 indicate antagonism, whereas a CI of 1 is indicative of additivism [60].

Cells were seeded at densities of 5.0×10^4 cells/well in 96 well plates as described in section 3.3. The cells were preincubated with the $cPLA_2\alpha$ inhibitors for two hours prior to treatment with BKM120. Cell viability was measured after 48 hours using the method described in section 3.3.

The experiment was repeated three times.

3.4 Flow cytometry

When flow cytometry was developed in the 1960's, its only application was counting and sorting of cells using a single parameter, whereas today, 14 parameters can be detected simultaneously [61, 62]. Flow cytometry use light scatter to characterise cells and cellular contents where physical properties, such as size, are described by the forward scatter (FS) of light. To characterise intracellular components, such as nucleic acids and proteins, fluorescent dyes are used. Antibodies conjugated to fluorescent dyes allow for the detection of specific proteins, either on the cell membrane or within the cell. Fluorochromes with similar excitation wavelength, but different emission wavelengths can be used in combination to measure several cell properties simultaneously [63].

Inside a flow cytometer, cells are suspended in a sheath fluid that ensures that the cells pass through the light beam, usually a laser, as single cells. As the cells pass through the light beam, light is scattered in all directions and is collected via optics that direct the light through a series of filters and dichroic mirrors that isolate particular wavelengths. The light signals are then detected by photomultiplier tubes and digitised for computer analyses [63].

3.4.1 Cell death assay

Cells undergoing apoptosis are under strict molecular control of caspases [35], and the presence of active caspases in cells can be used as a marker of apoptosis. CellEvent™ Caspase-3/7 Green Flow Cytometry Assay Kit (Thermo Fisher Scientific) was used to distinguish between live, apoptotic and necrotic cells. Active caspase-3/7 cleave the DNA binding dye in the Caspase-3/7 Green Detection Reagent and mark apoptotic cells with a bright fluorescent signal with excitation and emission maxima of 511 and 533

nm, respectively [64]. To differentiate between live and dead cells, SYTOX AADvanced dead stain was used. The complex of DNA and SYTOX has a fluorescent excitation and emission maxima of 546 and 647 nm, respectively [65]. When used in combination, the remaining cells that are not stained by either of the reagents are alive.

Following treatment with increasing concentrations of inhibitors, cells were stained according to the manufacturer's protocol [64]. The caspase detection reagent was detected in the FL1 channel with excitation 488 nm and emission 525 nm with bandpass (BP) 40 nm, whereas SYTOX was detected in the FL4 channel with the same excitation, but emission at 695 nm with BP 30 nm. A total of 20 000 cells were counted, and results were analysed using Kaluza.

3.4.2 Cell cycle analysis

To determine whether the relative viability achieved after treatment with inhibitors was a result of cell death or reduced proliferation, cell cycle assays were performed. The fluorescent dye propidium iodide (PI) bind stoichiometrically to nucleic acids and was used to quantify the DNA contents of cells, and further determine the cells' replication state [31, 35].

Cells were centrifuged at 1500 revolutions per minute (rpm) for 5 minutes and resuspended in freezer cold methanol previous to incubation for 10 minutes at -20°C to permeabilise the cell membrane for the stain. The samples were centrifuged at 1500 rpm for 5 minutes, and the supernatant discarded. 2 mL 200 µg/mL RNase was added to remove all the RNA in the sample. The samples were incubated for 30 minutes at room temperature (RT) before they were centrifuged at 1500 rpm for 5 minutes. The supernatant was discarded and the cells were stained with 1 mL 80 µg/mL PI in darkness at RT for 15 minutes and analysed in the flow cytometer.

When fixating cells, they tend to aggregate into bigger complexes consisting of multiple cells [66]. Complexes of multiple cells that pass the light beam in the flow cytometer will both have a larger FS and a longer time of flight

(TOF) compared to single cells. A dominant vertical population representing single cells became evident when TOF was plotted against FS. A gate was placed around this vertical population, preventing multiplets of cells to be analysed. During the process of fixating, some cells burst, and there will be aggregates of free DNA in the solution. To avoid that aggregates were analysed, a second gate was placed around the dominant population when FS was plotted against the fluorescence from PI. When combined, these two gates ensured that all events used in the analysis of replication state represented single cells.

3.5 Statistical analyses

In this thesis, a biological replica refers to repeated experiments using cells originating from a different cell culture flask. A technical replica refers to the repeated measurement of the same cell population. Wells with the same treatment in the same multiwell plate will be considered technical replicates. If the experiment is repeated three times with different cell populations, the plates will be considered as three biological replicates.

The relative fluorescent units (RFU) following viability assays were normalised to the mean of the control in each of the plates. Treatment effects were presented as relative viability, where the mean RFU of the control in respective experiments was considered to be 100%. All replicates, both technical and biological, were used to generate plots representing the effect of a given treatment. The plotted values were based on the average of all the normalised replicates for the given treatment ± SD, as achieved with GraphPad. Statistical significance between treatments were determined using Welch's ANOVA with Tamhane's T2 correction for multiple comparisons, $p < 0.05$ was considered statistically significant.

4 Results

4.1 Growth characteristics of the CCRF - CEM cell line

To determine the ideal window of growth and seeding conditions, the development in cell density over 7 days was investigated by cell counting and trypan blue exclusion (Figure 4.1). The determination of exponential growth phase was used to calculate the population doubling time (PDT).

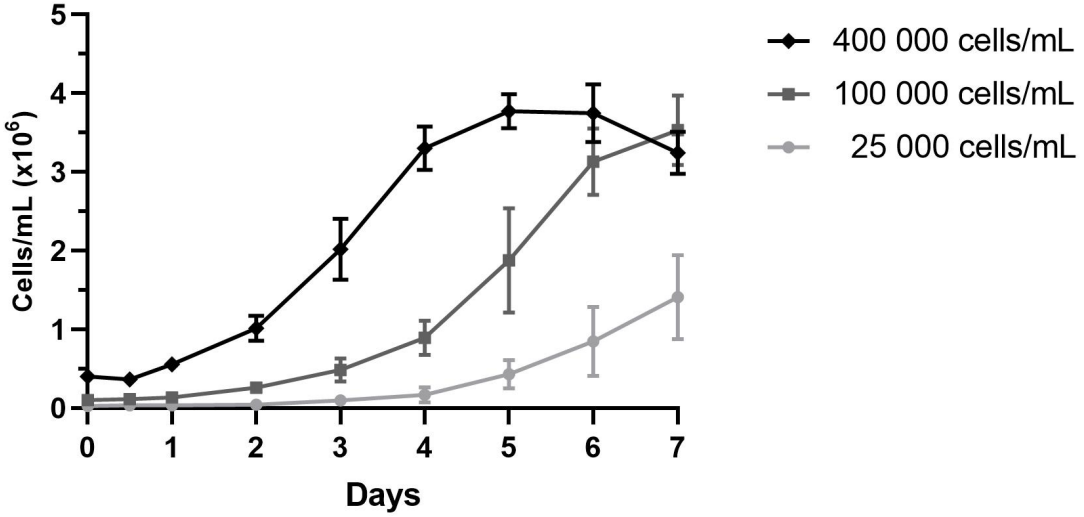

Figure 4.1: Growth curves of CCRF-CEM cells seeded at three different densities. Cells were counted from 12 hours to 7 days. The graph displays the mean cell densities ± SD from three biological replicates.

Cells seeded at the initial density of 2.5×10^4 cells/mL remained in lag phase for the duration of the experiment. Due to the great standard deviation between the biological replicates at days 6 and 7, it was not possible to assess whether the cells reached a true exponential growth phase starting at day 6, or if the increased proliferation observed at this time point was a result of variation between the biological replicates. Cells seeded at the density of 1.0×10^5 cells/mL reached an exponential growth phase at day 4, lasting until day 6 at which the growth slowed. The cells did not reach stationary phase. The great standard deviation at day 5 reflects the variation between the biological replicates. Lag, exponential and stationary phase

were observed for the cells seeded at 4.0×10^5 cells/mL. The cells displayed an exponential growth from day 2 until day 5, in which they entered death phase. The cell density continued to decrease from day 5 throughout the duration of the experiment.

Cells seeded at 2.5×10^4 cells/mL did not reach exponential growth phase, and the PDT could not be calculated. Cells seeded at 1.0×10^5 cells/mL had a PDT of approximately 27 hours, and cells seeded at 4.0×10^5 cells/mL had a PDT of approximately 30 hours (Table 4.1).

Table 4.1: Population doubling times (PDT) for the three cell densities cultured for the growth curve experiment. NA = not achieved.

Cell density (cells/mL)	PDT (h)
2.5×10^4	NA
1.0×10^5	26.5
4.0×10^5	29.6

From these results, it was determined that the optimal seeding density for the remaining cellular experiments were 4.0×10^5 cells/mL. This density allowed rapid, but controlled, entry into logarithmic growth without the risk of cell exhaustion and death.

4.2 CCRF - CEM cells are sensitive to cPLA$_2\alpha$ and PI3K inhibitors

Having determined the optimal growth conditions for the CCRF-CEM cells, our next aim was to investigate the effects of cPLA$_2\alpha$ inhibitors and the PI3K inhibitor BKM120 using the resazurin assay. Cells were treated for 24, 48 and 72 hours, in medium supplemented with both 0.5% (serum deprived) and 10% FBS to determine the best conditions for further experiments. Dose response curves were generated for all six conditions for the five inhibitors (Appendix D). The IC50 values are listed in Table 4.2.

When investigated in medium supplemented with 10% FBS, Compound 1 did not induce a dose dependent reduction in viability. It was therefore not possible to determine IC50 values under these conditions. However, when grown in serum deprived medium, cells treated with Compound 1 displayed

Table 4.2: IC50 values based on dose response curves displayed in Figures D.1–D.6. The cells were treated with the different inhibitors for 24, 48 and 72 hours in both medium supplemented with 10% and 0.5% FBS. NA indicate that it was impossible to fit a curve to the response after treatment with the inhibitor, and the IC50 values could not be determined.

Inhibitor	24 hours		48 hours		72 hours	
	0.5% FBS	10% FBS	0.5% FBS	10% FBS	0.5% FBS	10% FBS
Comp. 1	4.0 ± 0.4	NA	3.2 ± 0.3	NA	2.9 ± 0.3	NA
Comp. 2	7.6 ± 0.6	0.5 ± 0.1	5.5 ± 2.5	0.5 ± 0.02	0.6 ± 0.05	0.4 ± 0.01
Comp. 3	∼ 30	NA	NA	NA	∼ 30	NA
Comp. 4	9.2 ± 0.8	∼ 6	7.6 ± 0.9	NA	5.8 ± 0.5	NA
BKM120	∼ 18	∼ 6	0.9 ± 0.07	1.4 ± 0.05	1.0 ± 0.1	1.3 ± 0.05

a dose dependent reduction in viability. The IC50 values decreased with increasing treatment time, with IC50 values of 3.98 ± 0.5 µM, 3.13 ± 0.38 µM and 2.90 ± 0.5 µM after treatment for 24, 48 and 72 hours, respectively.

Compound 2 displayed a dose dependent reduction in viability under all the investigated conditions. Cells grown in medium supplemented with 10% FBS displayed similar IC50 values for all time points, with 0.5 ± 0.1 µM after 24 hours, 0.5 ± 0.002 µM after 48 hours and 0.6 ± 0.05 µM after 72 hours. In serum deprived medium, the IC50 was highest after 24 hours incubation, and decreased with increased treatment time with IC50 values of 7.6 ± 0.6 µM, 5.5 ± 2.5 µM and 0.6 ± 0.5 µM for 24, 48 and 72 hours, respectively. The dose response curve following treatment with Compound 2 for 48 hours in serum deprived medium (Figure D.4 C) does not display the normal sigmoid shape, which is reflected in the higher SD of the IC50 value (Figure D.4 C).

Compound 3 did not display a dose dependent reduction under any of the investigated conditions. In 10% FBS, only 0.12 µM and 30 µM gave a significant reduction in viability after treatment for 72 hours (Figure D.5 E). With serum deprivation, there was a trend of decreased viability at the highest concentrations of Compound 3. Although the viability was reduced

to approximately 50% when cells were treated with 30 µM of Compound 3 for 24 and 72 hours in serum deprived medium (Figures D.2 and D.6 C, respectively), it was not possible to generate a sigmoid dose response curve and the concentration cannot be considered a true IC50 value.

Similarly to treatment with Compound 1, IC50 values were not achieved when treatments with Compound 4 was given to cells in medium supplemented with 10% FBS. However, there was a clear trend of reduced viability after 48 and 72 hours when the cPLA$_2\alpha$ inhibitor was given in concentrations above 18 µM, but the viability did not result in 50% inhibition. After treatment with 6 µM of Compound 4 for 24 hours, the viability was reduced to approximately 50%. However, when Compound 4 was given in serum deprived medium, there was a dose dependent response for all three time points. The IC50 values were 9.2 ± 0.8 µM, 7.6 ± 0.9 µM and 5.8 ± 0.5 µM after 24, 48 and 72 hours, respectively.

The PI3K inhibitor BKM120 displayed dose dependent reduction in viability under all the six tested conditions. In medium supplemented with 10% FBS, the IC50 values were determined to be ∼ 6 µM, 1.4 ± 0.05 µM and 1.3 ± 0.05 µM after 24, 48 and 72 hours, respectively. The highest concentrations of 6 and 18 µM of BKM120 did not result in 50% inhibition after 24 hours, and it was therefore not possible to generate a sigmoid dose response curve to determine an exact IC50 value. This trend was also observed after 24 hours of treatment in serum deprived medium. In this case, the highest dose of 18 µM BKM120 resulted in 50% inhibition. The IC50 was determined to be 0.9 ± 0.07 µM and 1.0 ± 0.1 µM after 48 and 72 hours, respectively.

Collectively, dose dependent inhibition was found for Compounds 1, 2 and 4 and BKM120, but not for Compound 3. The inhibition was also found to be time dependent, with increasing inhibition over time. Interestingly, the concentration of serum had contrasting effects on inhibition. Compound 2 worked best in medium supplemented with 10% FBS, whereas Compounds 1 and 3, and BKM120 worked better in medium supplemented with 0.5% FBS.

4.3 Combinations between Compounds 1 and 2 with BKM120 have a synergistic effect on viability

Combination therapies represent an advantageous line of action compared to monotherapies due to the potential for synergy and reduced adverse side effects for patients, as previously mentioned (Section 3.3.1). Previous work performed in this laboratory has indicated synergy between Compound 1 and BKM120 in various other cell lines (unpublished results), and it was therefore decided to investigate the combination of cPLA$_2\alpha$ and PI3K inhibitors also in the CCRF-CEM cell line. Based on the established dose and time dependency for Compounds 1 and 2 and BKM120, a number of combination experiments were performed. Suboptimal doses of each compound, typically corresponding to 10 - 20% inhibition of viability, were used to investigate possible synergy. In Table 4.3 and Table 4.4, inhibition is presented as reduction in viability determined by the resazurin assay, with corresponding combination index (CI) for selected combinations of low dose BKM120 with Compound 1 and Compound 2, respectively. Significance denotes the significance level of the difference between the combination treatment and the respective monotherapies of BKM120 and Compounds 1 and 2. The effects of the inhibitors as monotherapies are presented in Tables E.1–E.4 in Appendix E.

When assessing the CIs in Table 4.3, all the tested combinations of low dose BKM120 and Compound 1 seem to indicate synergy as the CI values are less than 1. However, when comparing the reduction in viability following the combination treatments to the respective monotherapies, it becomes evident that this is not the complete picture. None of the combination therapies with 0.5 µM of BKM120 and Compound 1 were statistically significant from their respective monotherapies of Compound 1. The inhibitors are therefore not considered to act in synergy within this concentration interval. The reduction in viability for the combination treatments with 0.6 µM of BKM120 and Compound 1 were statistically significant from the inhibitory effect of the respective monotherapies, and the inhibitors were thus found to act in synergy within this interval.

Table 4.3: Total inhibition for the combinations of BKM120 (µM) and Compound 1 (µM) presented as the mean ± SD with corresponding combination index (CI). The significance denotes significance between the combination treatment and the respective monotherapy. Comp. 1 = Compound 1, NS = non significant, * = p <0.05, ** = p <0.01, *** = p <0.001, ◆ = p <0.0001.

				Significance	
BKM120	Comp. 1	Total inhibition	CI	BKM120	Comp. 1
0.5	2.2	22.7 ± 10.4	0.91	***	NS
0.5	2.4	28.2 ± 8.1	0.85	◆	NS
0.5	2.6	39.8 ± 7.2	0.92	◆	NS
0.6	2.0	30.8 ± 7.8	0.81	◆	◆
0.6	2.2	33.8 ± 9.9	0.94	◆	*
0.6	2.4	42.3 ± 7.1	0.82	◆	***

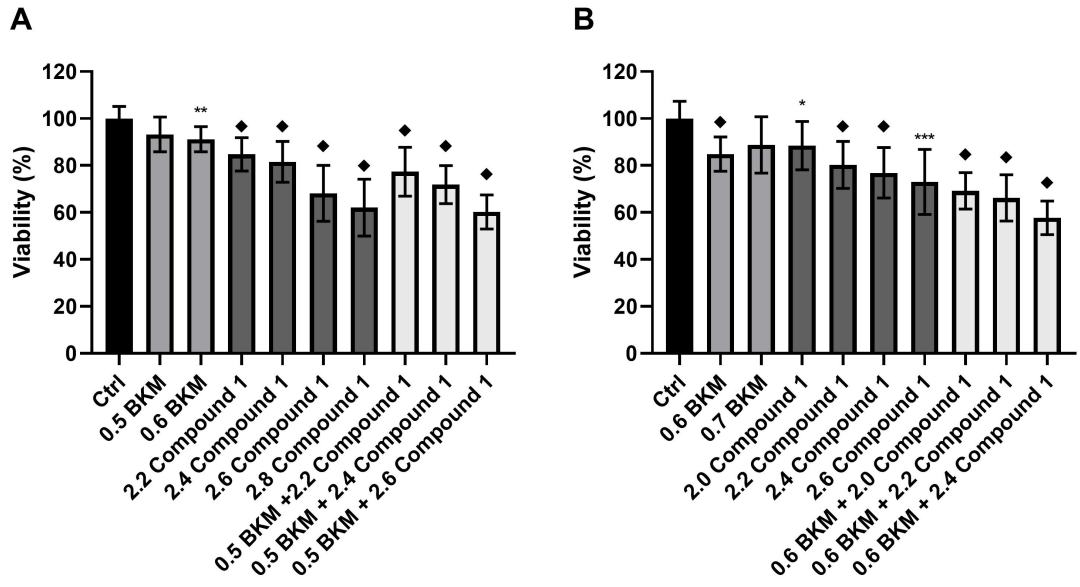

Figure 4.2: Combination treatment of BKM120 (µM) and Compound 1 (µM). The bars represent the mean relative viability ± SD of three biological replicates. In A, the low dose of BKM120 used in combination corresponds to an expected inhibition of 10%, whereas in B the low dose BKM120 is expected to give a 15% reduction in viability. Ctrl = control treatment, set to 100% viability. * = p <0.05, ** = p <0.01, *** = p <0.001, ◆ = p <0.0001.

Table 4.4: Total inhibition for the combinations of BKM120 (µM) and Compound 2 (µM) presented as the mean ± SD with corresponding combination index (CI). The significance denotes significance between the combination treatment and the respective monotherapy. Comp. 1 = Compound 1, NS = non significant, * = p <0.05, ** = p <0.01, *** = p <0.001, ◆ = p <0.0001.

				Significance	
BKM120	Comp. 2	Total inhibition	CI	BKM120	Comp. 2
0.5	0.16	21.8 ± 6.8	0.74	◆	◆
0.5	0.20	26.4 ± 4.9	0.80	◆	**
0.5	0.24	37.5 ± 7.2	0.62	◆	◆
0.6	0.12	21.7 ± 11.1	0.78	NS	NS
0.6	0.16	22.7 ± 13.1	0.75	NS	*
0.6	0.20	30.3 ± 9.4	0.66	◆	***

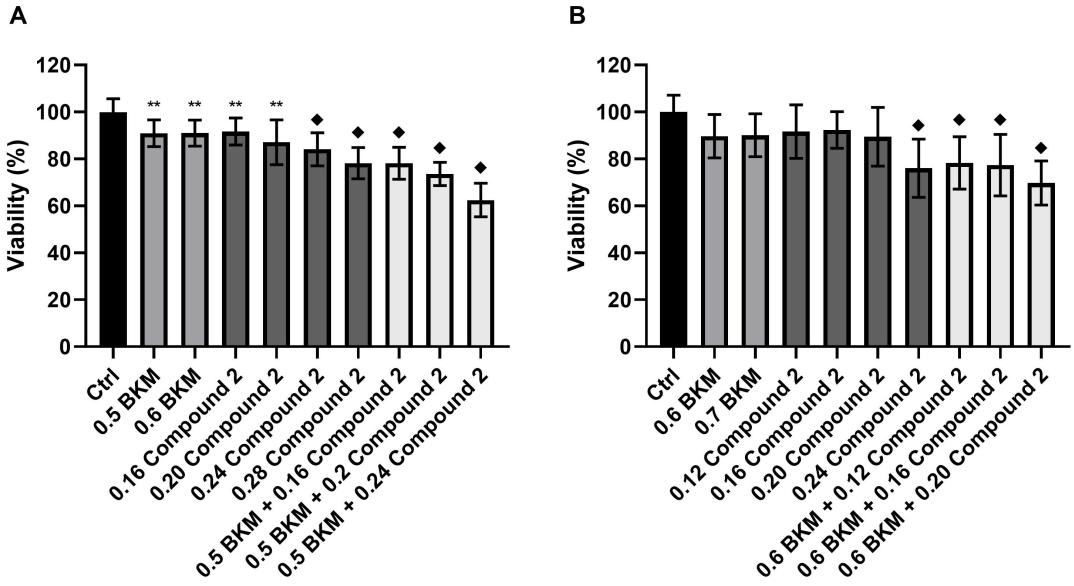

Figure 4.3: Combination treatment of BKM120 (µM) and Compound 2 (µM). The bars represent the mean relative viability ± SD of three biological replicates. In A, the low dose of BKM120 used in combination corresponds to an expected inhibition of 10%, whereas in B the low dose BKM120 is expected to give a 15% reduction in viability. Ctrl = control treatment, set to 100% viability. * = p <0.05, ** = p <0.01, *** = p <0.001, ◆ = p <0.0001.

As indicated by the low CIs in Table 4.4, the combinations of BKM120 and Compound 2 displayed a synergistic mechanism. The reduction in viability for all six combinations between BKM120 and Compound 2 were statistically significant from the untreated control. However, when comparing the viability of the combination treatments with 0.6 µM of BKM120 and Compound 2 with the respective monotherapies, the reduction in viability was not found significant with the exception of the highest combination of Compound 2. The combinations with 0.6 µM of BKM120 and Compound 2 were thus not considered to display a synergistic mechanism.

Dose dependent inhibition was found for all the investigated combinations of Compounds 1 and 2 with BKM120. Based on the CI values alone, the compounds were found to act in synergy. After considering the difference between the combination therapy and the respective monotherapies, only half the combinations were statistically significant. Compound 1 was found to act in synergy with 0.6 µM of BKM120, whereas Compound 2 acted in synergy with 0.5 µM of BKM120.

4.4 cPLA$_2$α inhibitors induce apoptosis and necrosis in a serum dependent manner

The previous resazurin assays showed that the cPLA$_2$α inhibitors Compounds 1, 2 and 4 and the PI3K inhibitor BKM120 reduced viability in a dose dependent manner. A cell death assay using flow cytometry was performed to verify these findings, in addition to classify the mechanism of cell death as either apoptosis or necrosis. The effect of inhibitors were investigated under optimal serum condition, as determined by the resazurin assay. BKM120 only displayed minor differences in IC50 values with 10% FBS and 0.5% FBS, and both serum concentrations were therefore investigated. Figures 4.4 and 4.5 display the distribution of necrotic, apoptotic and live cells after treatment with increasing concentration of inhibitors in medium supplemented with 0.5% FBS and 10% FBS, respectively. Density plots for selected treatments with gates are depicted in Figure 4.6.

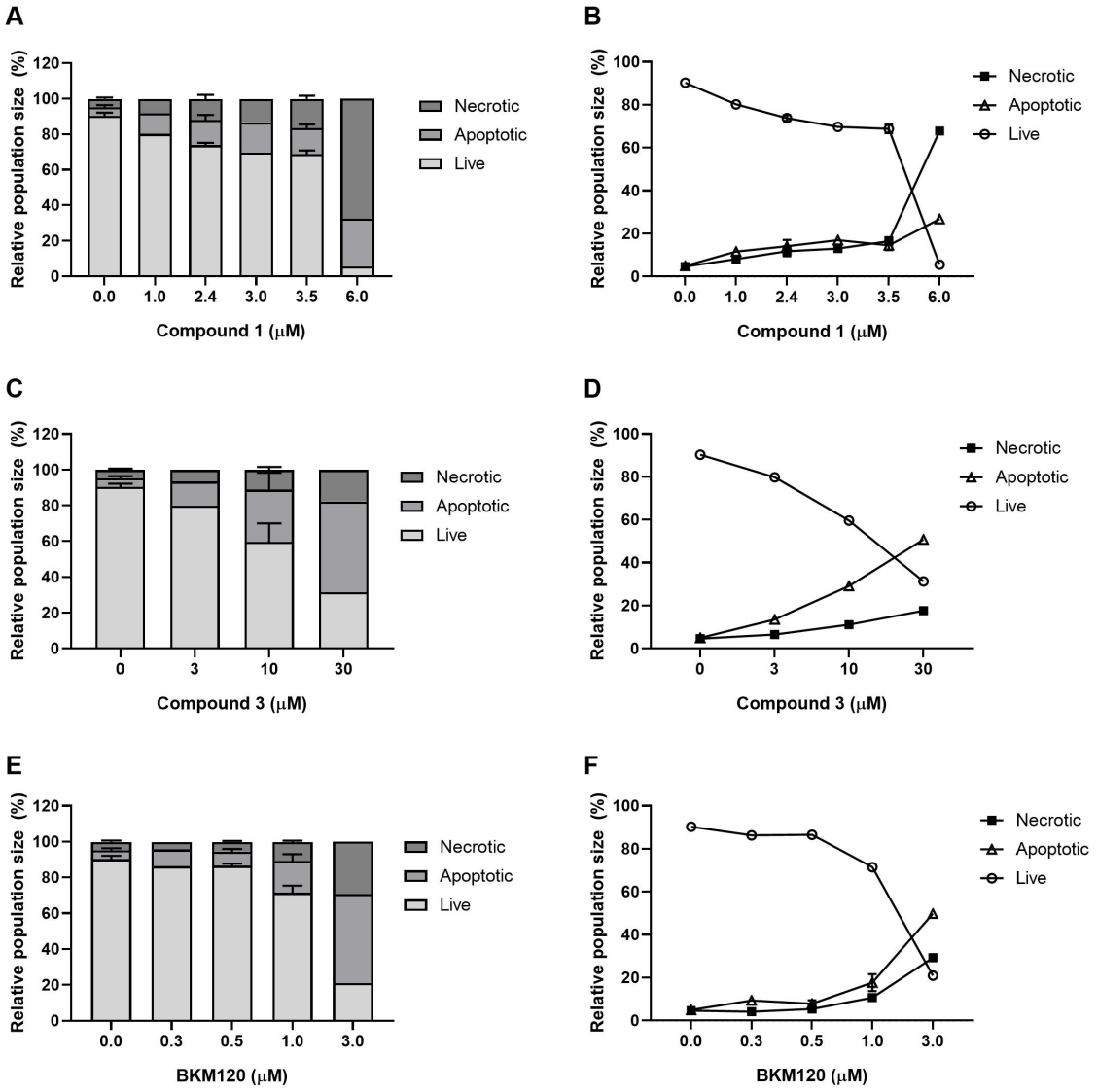

Figure 4.4: CellEvent Caspase-3/7 Green Flow Cytometry Assay Kit was used to distinguish living, apoptotic and necrotic cells after 48 hours of treatment in serum deprived medium, represented as relative population sizes of the total number of analysed cells. Cells treated with 1 - 6 µM Compound 1 are shown in A and B, 3 - 30 µM Compound 3 in C and D and 0.3 - 3 µM BKM120 in E and F. The concentrations with error bars represent the mean of three biological replicates ± SD, whereas the bars without error bars represent one biological replicate.

The viable populations decreased with increasing concentrations of Compounds 1 and 3 and BKM120 in medium supplemented with 0.5% FBS (Figure 4.4), confirming a dose dependent relationship between viability and inhibitors. For Compound 3 and BKM120, the sizes of the necrotic populations were relatively stable across the increased inhibitor concentrations, indicating that the inhibitors predominantly induced apoptosis. This was also evident by the presence of a dominating apoptotic population at the highest treatment doses of 30 µM of Compound 3 and 3 µM of BKM120. For Compound 1, the highest concentration of 6 µM induced necrosis. At the lower concentrations, the apoptotic and necrotic populations were approximately of the same size.

In medium supplemented with 10% FBS, there was no difference between induction of necrosis or apoptosis after treatment with Compound 2 and BKM120 (Figure 4.5). There was, however, a dose dependent reduction of the viable population with increasing concentration of inhibitor, verifying the obtained results of dose dependency in the resazurin assay.

Interestingly, there was a difference in the response pattern after treatment with BKM120, depending on the serum concentration in the medium. There were approximately 20% viable cells after treatment with 3 µM of BKM120 in serum deprived medium (Figure 4.4 E and F), compared to approximately 8% in medium supplemented with 10% FBS (Figure 4.5 C and D). In serum deprived medium, the necrotic population was greater than the apoptotic for all concentrations of BKM120, whereas these populations were of the same size in 10% FBS, regardless of the inhibitor concentration.

Furthermore, Compound 3 displayed a dose dependent reduction in viability with a viable population of 20% after treatment with 30 µM of the inhibitor. This effect was not observed in the resazurin assay, indicating that the cell death assay using flow cytometry was a more sensitive method for analysis.

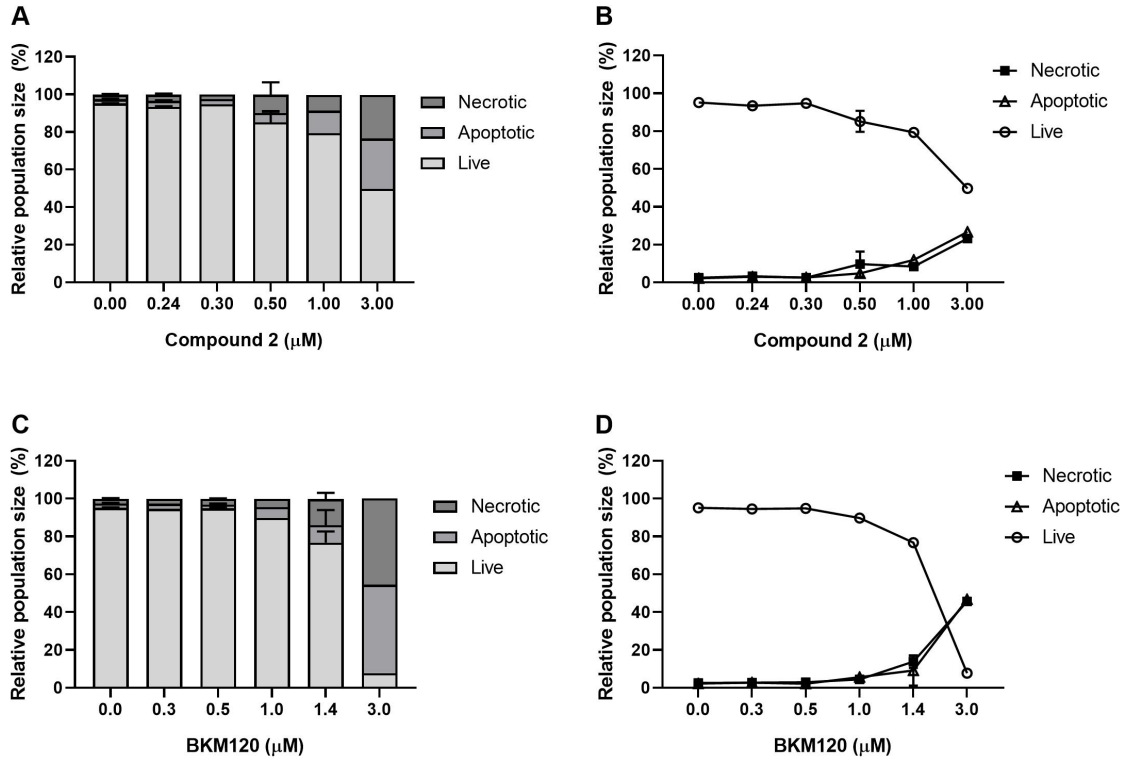

Figure 4.5: CellEvent Caspase-3/7 Green Flow Cytometry Assay Kit was used to distinguish living, apoptotic and necrotic cells after 48 hours of treatment in 10% FBS, represented as relative population sizes of the total number of analysed cells. Cells treated with 0.24 - 3 µM Compound 1 are shown in A and B and 0.3 - 3 µM BKM120 in C and D. The concentrations with error bars represent the mean of three biological replicates ± SD, whereas the bars without error bars represent one biological replicate.

At the lower inhibitor concentrations, the apoptotic and necrotic populations were easily distinguishable (Figure 4.6). However, after treatment with the highest doses of Compound 1 and BKM120, a tail between the apoptotic and necrotic population became present. This tail represents cells that were transitioning from a controlled death through apoptosis to sudden death through necrosis.

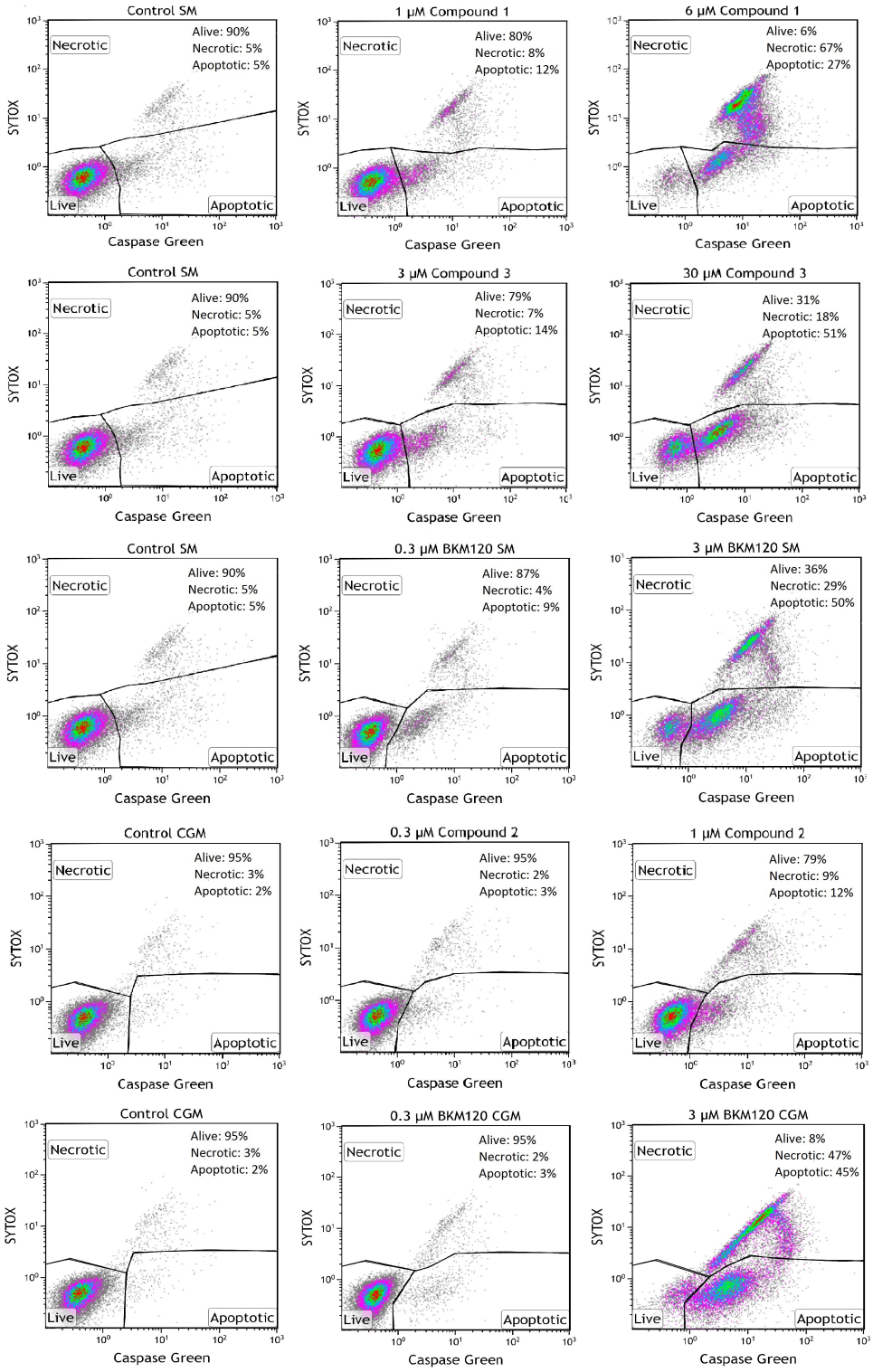

Figure 4.6: Density plots representing high and low doses for the investigated inhibitors, with gates for determination of the sizes of the living, necrotic and apoptotic population. The percentages given in each subfigure is representing the number of cells in that population, based on the total number of cells in the analyses. No normalisation has been performed. SM = Starvation medium with 0.5% FBS, CGM = Complete growth medium with 10% FBS.

4.5 Inhibition of cPLA$_2\alpha$ does not affect cell cycle progression

Even if treatment with an inhibitor does not cause reduction in viability, it does not mean that the inhibitor is without an effect in the given cell line model. It could be that the inhibitor is exerting its effect on other mechanisms that do not influence viability, such as cell cycle arrest. In these cases, the cells are retained at one of the checkpoints in the cell cycle. As the cells remain alive, the effect of the inhibitor cannot be detected by viability assays. To investigate whether some of the inhibitors caused cell cycle arrest, cells were fixed after treatment with inhibitors and stained with PI that binds nucleic acids stoichiometrically. The fluorescence from PI was detected using flow cytometry and quantified in Kaluza.

There were minor differences in the distribution of cells in the different phases of the cell cycle after treating the cells for 48 hours under serum deprivation (Figure 4.7). Approximately 50% of the cells were in G_1 after treatment with Compound 1, regardless of concentration (Figure 4.7 A and B). Cells treated with 2.4 µM of Compound 1 displayed the greatest deviation from the control, with an increased population of cells in G_1, and decreased populations in S and G_2 + M phases. The same trend was observed in cells treated with Compound 3 (Figure 4.7 C and D). The minor variation between treatments were considered to be caused by technical discrepancy, rather than biological effects. As there was only one biological replicate for treatment with 3 and 30 µM of Compound 3, it is not possible to perform statistical analyses on the distribution of cells in the different phases of the cell cycle. Following treatment with BKM120, approximately 50% of the cells were found in G_1 (Figure 4.4 E and F). It was only the highest concentration of 3 µM BKM120 that altered the distribution of cells in the different phases of the cell cycle, in which cells were retained in the S phase on the expense of G_1 phase.

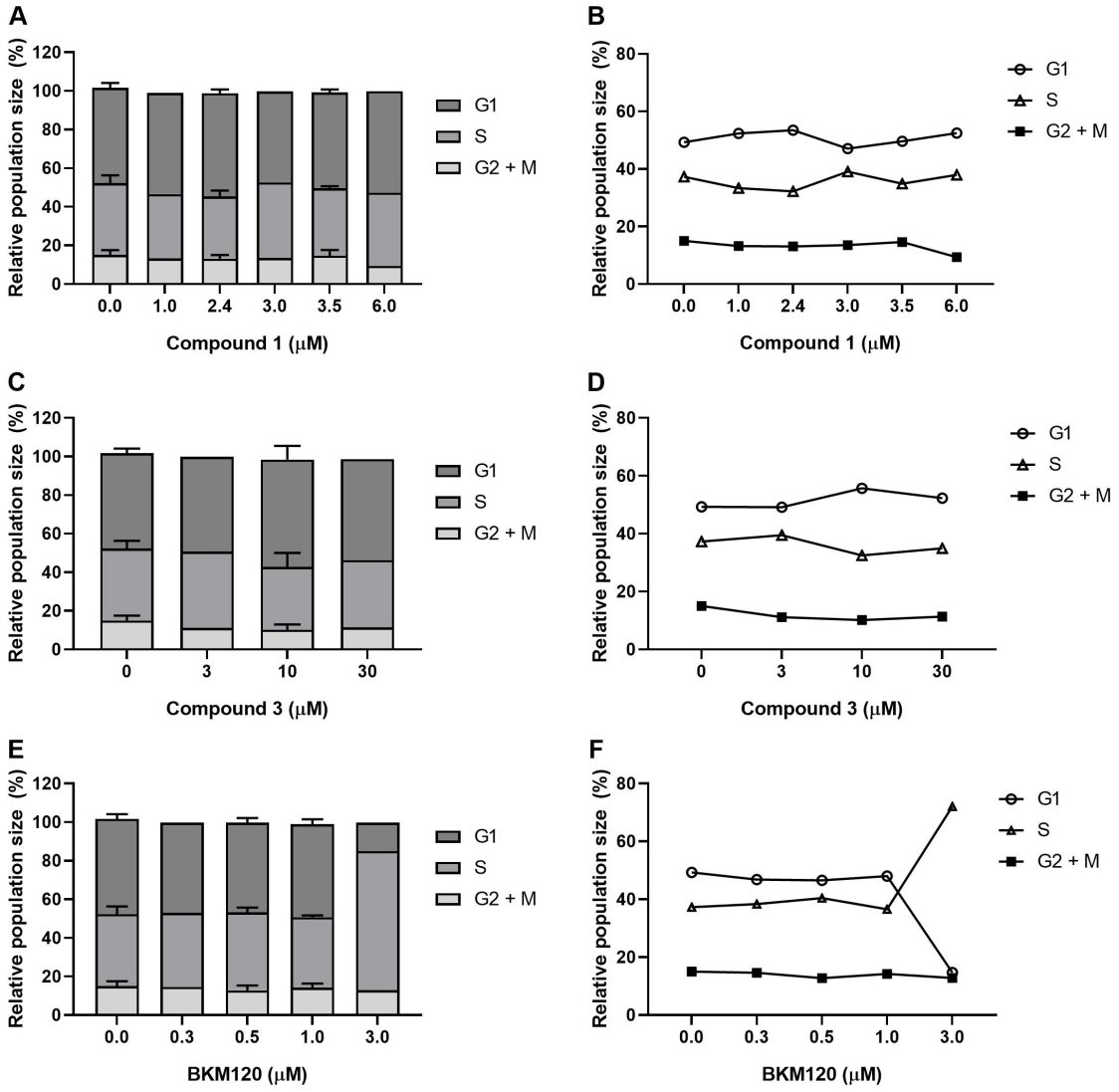

Figure 4.7: The DNA contents of fixed cells were quantified using propidium iodide (PI) after 48 hours of treatment in serum deprived medium. The graphs and plots are based on gated histograms with the number of counted cells plotted against fluorescence of PI. Cell populations in the different phases of the cell cycle are relative to the total number of analysed cells. Cells treated with 1 - 6 µM Compound 1 are shown in A and B, 3 - 30 µM Compound 3 in C and D and 0.3 - 3 µM BKM120 in E and F. The concentrations with error bars represent the mean of three biological replicates ± SD, whereas the bars without error bars represent one biological replicate.

The distribution of cells in the different phases of the cell cycle after treatment with Compound 2 and BKM120 for 48 hours in medium supplemented with 10% FBS is depicted in Figure 4.8. There was a trend of increased populations in the S and G_2 + M phases with increasing concentrations of

Compound 2, indicating a dose dependent retention in these phases of the cell cycle (Figure 4.8 A and B). At the highest concentration of 3 µM of Compound 2, the G_1 population was halved compared to the control. The remaining cells were evenly distributed in the S and G_2 + M phases, as indicated by the overlapping lines. The same trend was evident in cells treated with BKM120 (Figure 4.8 C and D). The population of G_1 cells was reduced to approximately 7% after treatment with 3 µM of BKM120, compared to 95% in the control. As for Compound 2, the remaining cells not in G_1 phase after treatment with BKM120 were evenly distributed in the S and G_2 + M phases.

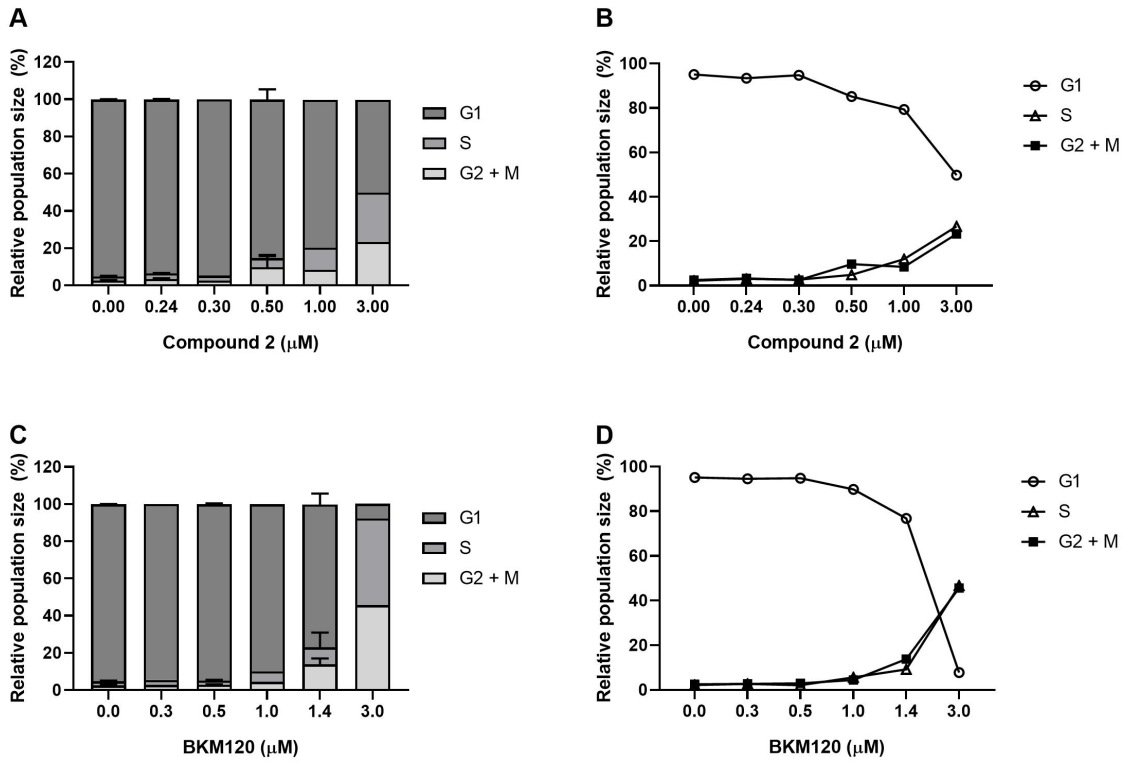

Figure 4.8: The DNA contents of fixed cells were quantified using propidium iodide (PI) after 48 hours of treatment in CGM. The graphs and plots are based on gated histograms with the number of counted cells plotted against fluorescence of PI. Cell populations in the different phases of the cell cycle are relative to the total number of analysed cells. Cells treated with 0.24 - 3 µM Compound 1 are shown in A and B and 0.3 - 3 µM BKM120 in C and D. The concentrations with error bars represent the mean of three biological replicates ± SD, whereas the bars without error bars represent one biological replicate.

In total, there were bigger differences between the S and G_2 + M phases

in the untreated control under serum deprivation, compared to medium supplemented with 10% FBS. In medium supplemented with 0.5% FBS, approximately 15% of the cells were in G_2 + M and 40% in S phase. These phases were almost not detectable in medium supplemented with 10% FBS in which 95% of the cells were in the G_1 phase, and the remaining 5% were equally distributed between the S and G_2 + M phases. In medium supplemented with 0.5% FBS, it was only 3 µM BKM120 that induced a retention in S phase of the cell cycle. The other treatments did not affect the cells' progression through the cell cycle. Treatments with both Compound 2 and BKM120 given in medium supplemented with 10% FBS gave a dose dependent retention of cells in the S and G_2 + M phases of the cell cycle compared to the control. However, due to the unlikely distribution of cells in the different phases of the cell cycle in the control treatment in medium supplemented with 10% FBS, these results are considered invalid.

5 Discussion

5.1 Growth characteristics and morphological traits of CCRF - CEM cells

The cell line of CCRF-CEM has served as model system to investigate the role of cPLA$_2\alpha$ as a possible therapeutic target in the context of T-ALL. Prior to any experiments with inhibitors, growth curves and observations of morphology were made. Only the highest cell density of 4.0×10^5 cells/mL displayed lag, exponential and stationary phase (Figure 4.1). This cell density also displayed the overall lowest SD across biological replicates, allowing the most accurate determination of population doubling time (PDT) and more reliable growth predictions prior to experiments.

The PDT was approximately 3 hours longer for the highest cell density of 4.0×10^5 cells/mL compared to the intermediate cell density of 1.0×10^5 cells/mL. This might be a result of unsuccessful seeding of the cells, but most likely a consequence of serum depletion as no fresh medium was added throughout the experiment. According to the supplier, it is recommended to add fresh medium with 10% FBS every 2 - 3 days [54]. The serum contains important growth and survival factors [67], and these might have become a limiting factor during the exponential growth phase, reducing the proliferative rate.

Under standard conditions between experiments, the CCRF-CEM cells displayed a normal lymphoblastic morphology (Section 1.3.2). However, immediately after establishment of the culture from cryopreservation, the cells displayed an inconsistent morphology where the cells were bigger and more rugged than normal lymphoblasts. After approximately 30 passages, the cells displayed an altered growth pattern and morphology. The proliferation suddenly increased, and was no longer predictable. Furthermore, the cells became significantly smaller, which is consistent with a reduced growth period prior to cell division. To ensure credibility of the experiments, cells were discarded after 25 passages.

5.2 cPLA$_2\alpha$ inhibitors in regulation of cell death and survival

The activation of cPLA$_2\alpha$ by tumour necrosis factor (TNF) has been shown to be an important element in the signalling pathway leading to cell death in multiple human leukaemic cell lines [68]. However, several of these cell lines, including CCRF-CEM, are resistant to TNF induced cell death, and thus render them resistant to drugs that trigger the intrinsic pathway of apoptosis [68, 69]. Downstream effects of the eicosanoid production by cPLA$_2\alpha$ include increased proliferation and survival. Therefore, we wanted to study the effect of inhibiting cPLA$_2\alpha$ and investigate whether this could affect the survival of cancer cells.

Dose and time dependency of inhibitors in the regulation of viability were established using resazurin in CCRF-CEM cells. The redox dye is not a specific analysis of viability, but rather a measurement of the metabolic activity in the cells [56]. However, observations of morphological changes of the cells after treatment with inhibitors were consistent with that of dying cells. It was therefore concluded that the observed reduction in metabolic activity was a result of reduced viability.

Cells treated with Compounds 1, 2 and 4 and BKM120 displayed a dose dependent reduction in viability. Compounds 1 and 4 did only exert an effect on viability in serum deprived medium, whereas Compound 2 and BKM120 exerted their effect in both serum concentrations. However, Compound 2 displayed lower IC50 values in medium supplemented with 10% FBS, while BKM120 worked best with serum deprivation. Treatment with Compound 3 did not display a dose dependent reduction in viability as assessed with resazurin. This is consistent with the findings in similar experiments performed in other cell lines at the laboratory. However, a dose dependent reduction in viability was observed after using the CellEvent flow cytometry kit. This suggests that the resazurin assay is not sufficiently sensitive to detect the effects of Compound 3, which should be taken into consideration in future experiments regarding the resazurin assay.

The cPLA$_2\alpha$ inhibitors used in these studies are known to target the enzyme specifically and reduce the production of arachidonic acid through reversible competitive binding of the active site (Personal communication with Prof. Berit Johansen, Trondheim 22.03.2019). In summary, all four of the tested cPLA$_2\alpha$ inhibitors resulted in a reduction in viability, suggesting that arachidonic acid and its derivatives affect signalling networks involved in the regulation of cell death and survival.

5.3 Assessment of synergy by resazurin

Synergy between drugs pose an advantageous therapeutic strategy in cancer treatment. There are several ways to assess the combination of multiple compounds as synergism, additivism or antagonism [60, 70]. It is not one method that can be applied to all situations, and there are therefore several considerations to be aware of when seeking to identify synergy. The most commonly used approach is the Chou-Talalay method based on the mass-law principle and enzyme kinetics, whereas Bliss Independence is typically used when the specific drugs have different sites of action in the cell [60, 71, 72]. As the inhibitors used in combination target two different enzymes, synergy was determined using a combination index (CI) calculated using Bliss Independence. This approach allowed the determination of quantifiable values of synergy, and made it possible to ascertain the mode of action of the combination treatment.

A CI of less than 1 indicates that the combination of compounds is more effective than the additive effect of the compounds given as monotherapies, and thus act in synergy. Based on the CIs alone, Compounds 1 and 2 acted in synergy with BKM120 when given in suboptimal concentrations. However, when performing statistical analyses on the viability data, where the combination treatment was compared to the respective monotherapies, several of the combinations were non significant. This indicates that Bliss Independence alone in this case is insufficient to determine synergy based on resazurin assay. In the calculation of the CIs, the mean effects of the treatments were used, without taking the SD into consideration. The non

significant difference in treatment effects between the combination treatments and the respective monotherapies is caused by the high SDs in the measurement of viability, as seen in Tables 4.3 and 4.4. This suggest that the measurements of inhibition by resazurin is not sufficiently accurate to quantify synergy with Bliss Independence.

It is important to keep in mind that even though specific combinations of suboptimal concentrations of two compounds are indicative of synergy, it does not mean that the drugs always act in synergy. It simply means that the compounds will have concentration intervals in which they act in synergy. Moreover, if concentrations outside of these intervals are used, the compounds may display antagonism rather than synergy [60].

5.4 The induction of apoptosis and necrosis is serum dependent

Foetal bovine serum (FBS) is one of the most used growth supplements for cell culture, primarily because of its high concentration of factors that stimulate growth and survival [73]. Kume *et al.* report that an acid of low molecular weight derived from FBS inhibited the activation of Caspase-3 in rat primary culture of cortical neurons and thereby preventing cell death in treatment previously shown to induce cell death [74]. Under normal circumstances in cell cultivation, factors promoting survival and growth contribute to the maintenance of homeostasis in the cell culture. However, during *in vitro* experiments aiming to reduce viability, such factors might counteract the treatment effects. Therefore, to ensure the integrity of the death assays, treatments were conducted in both serum deprived medium and medium supplemented with 10% FBS to investigate the mode of death following inhibition of $cPLA_2\alpha$ and PI3K.

Treatment with 6 µM of Compound 1 predominantly induced necrosis, as the necrotic population was approximately two fold bigger than the apoptotic. This treatment corresponds to roughly twice the IC50 dose after 48 hours in serum deprived medium as determined in the resazurin assay. It

was therefore expected to observe a substantial amount of cell death. During the process of necrosis, cells excrete stress signals and by that induce necrosis in surrounding cells. The vast induction of necrosis might therefore be a result of a wave of death signals from other necrotic cells, and not due to the specific inhibition of cPLA$_2\alpha$. This is supported by the presence of a tail of cells connecting the apoptotic and necrotic population (Figure 4.6). This tail was also observed after treatment with 3 µM of BKM120, but considerably smaller. The tail represent cells transitioning from a controlled cell death to a sudden and abrupt death through necrosis. The necrotic population is therefore likely to be somewhat smaller than reported. Furthermore, the necrotic and apoptotic populations were of the same size after treatment with lower doses of Compound 1, suggesting that the dramatic increase in the necrotic population was caused by a shock wave of necrotic death signals.

Compound 1 is both hydrophobic and lipid like, and the increased necrosis observed after treatment with 6 µM of Compound 1 might therefore be a result of lipotoxicity, rather than specific inhibition of cPLA$_2\alpha$. Engin defines lipotoxicity as *"deleterious effects of lipid accumulation in non-adipose tissues"* [75]. The effects of lipotoxicity is hence not limited to a single mechanism, but a collection of destructive effects. Compounds 2 and 3, on the other hand, are just hydrophobic and do not share the lipid like characteristics of Compound 2 (Personal communication with Prof. Berit Johansen, Trondheim 09.05.2019). Compound 2 did not differentiate between either mode of death, as the apoptotic and necrotic populations were of the same size (Figure 4.5 B), whereas Compound 3 predominantly induced apoptosis (Figure 4.4 D). Compounds 1 and 3 have the same target, and it was therefore expected that they induced the same mode of death under the same experimental conditions. Since all the other experimental factors were identical, the observed difference in mode of death for Compound 1 and 3 can be assigned to the lipid like characteristics of Compound 1.

Treatment with BKM120 in serum deprived medium preferentially induced apoptosis, whereas the induction of death in medium supplemented with

10% FBS was unbiased. The cells received identical treatment, suggesting that the mode of death was serum dependent. Serum concentration has proven to affect viability, and it is therefore not unlikely that it also affect mode of death.

5.5 cPLA$_2\alpha$ in regulation of cell cycle progression

Several studies have implied that cPLA$_2\alpha$ is a regulator of cell cycle progression [76–78]. Naini *et al.* report that the regulatory effect of cPLA$_2\alpha$ is independent of its phospholipase activity and Muckova *et al.* propose that cPLA$_2\alpha$ interact with regulators of the cell cycle through its C2 domain [76, 77]. It was therefore not expected to observe any changes in cell cycle progression after treating the cells with Compounds 1, 2 and 3 as these are specifically inhibiting the phospholipase activity through reversible binding to the active site.

Approximately 50% of the cells were in G_1 phase after treatment with Compounds 1 and 3 in serum deprived medium, regardless of the inhibitor concentration (Figure 4.7). The remaining cells were evenly distributed in the S and G_2 + M phases. This was consistent with the expected distribution of cells in the cell cycle phases as displayed in Figure 1.4. The inhibitors were therefore not affecting the cell cycle progression in serum deprived medium.

In medium supplemented with 10% FBS, 95% of the control cells were found in the G_1 phase. This is in conflict with the expected distribution of cells in the cell cycle. It is therefore suspected that the experimental design measuring the cell cycle progression in medium supplemented with 10% FBS was flawed. The retention of cells in S and G_2 + M following treatment with 3 µM of Compound 2 and BKM120 is thus considered invalid. These treatments were also only tested once, and the experiment must be repeated and optimised to attain reliable results in medium supplemented with 10% FBS.

The absent effects of cPLA$_2\alpha$ inhibitors on cell cycle progression is in line with other studies [76–78]. Furthermore, these data supports that Compounds 1 and 3 binds specifically to the active site of the enzyme, without affecting its physical properties.

5.6 cPLA$_2\alpha$ as a therapeutic target in T - ALL

Cancer cells arise as a consequence of multiple mutations that favour both uncontrolled cell division and reduce the cells' susceptibility for cell death. These mutations alter the balance of survival and death signals, rendering the cancer cells reliant on these specific signalling patterns [3, 5, 79]. Targeting central nodes in the signalling network will disrupt the delicate balance, with fatal consequences for the cancer cells [80].

From both the resazurin assays and investigation of mode of death, it was evident that the specific inhibition of cPLA$_2\alpha$ reduced viability of CCRF-CEM cells, however through unknown mechanisms. Prostaglandin E_2 (PGE_2) derived from the COX pathway and leukotriene B_4 (LTB_4) from the LOX pathway are eicosanoids known to activate several signalling pathways involved in cell survival, proliferation, and invasion and migration of cancer cells (Figure 5.1) [47, 53, 81]. We therefore suggest that the reduction in viability was a result of reduced levels of eicosanoids in the cells.

Lipid mediators, such as PGE_2 and LTB_4, act in paracrine and autocrine manners, conferring signals for proliferation and survival to surrounding cells. In addition to create a tumour promoting microenvironment, prostaglandins and leukotrienes also activate stromal cells. Upon activation, these cells migrate towards the tumour cells where they secrete factors stimulating growth and angiogenesis [81]. In combination with the autocrine and paracrine stimulation of cell survival and proliferation by eicosanoids, these factors enhance the invasion of cancer cells into the surrounding tissues [53, 81].

CCRF-CEM cells have an activating mutation of the oncogene KRAS [82, 83]. As a result, the GTPase gene product k-Ras display prolonged acti-

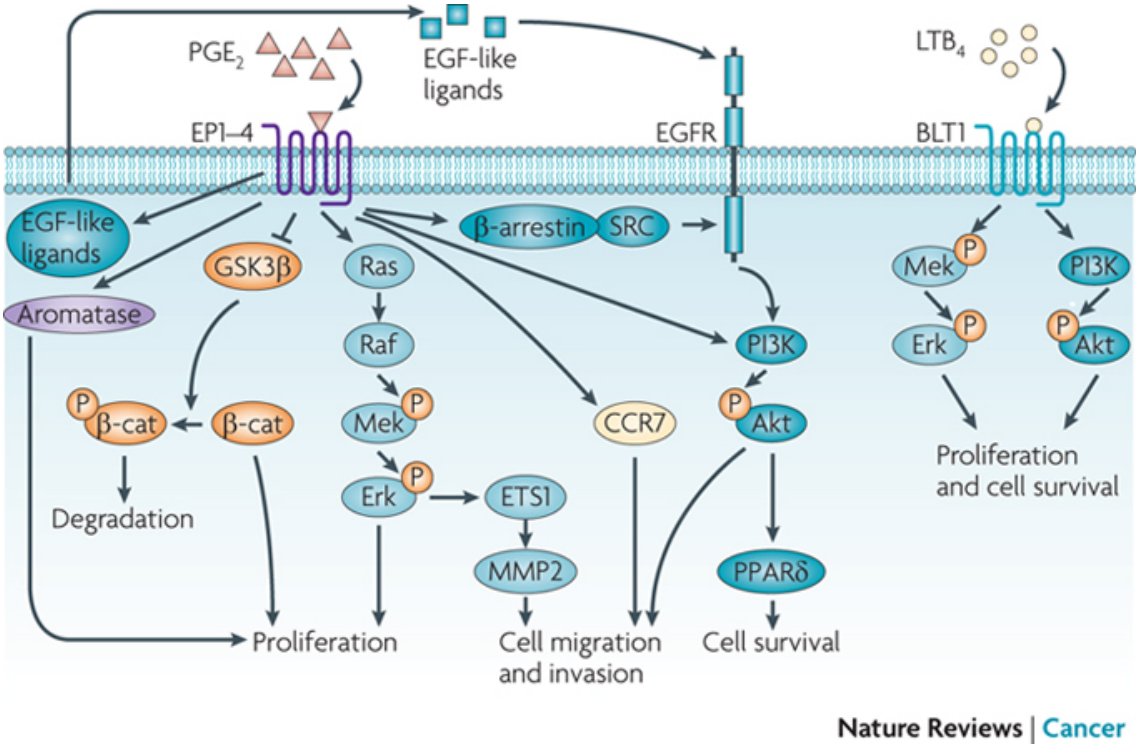

Figure 5.1: Bioactive lipids derived from arachidonic acid have crucial roles in both chronic inflammation and cancer. The metabolism of arachidonic acid by cyclooxygenase and lipoxygenase pathways produce prostaglandins and leukotrienes, respectively. These eicosanoids promote cancer progression through induction of cell survival, proliferation, migration and invasion. PGE_2 promotes cell survival by activating the PI3K/Akt pathway, in addition to induce proliferation and cell migration and invasion through Erk. LTB_4 stimulate cell proliferation and promote cell survival through Mek/Erk and PI3K/Akt pathways [53]. Figure from Wang & Dubois with permission [53].

vation upon stimulation and thus increase proliferation and cell migration and invasion [53, 83]. Chan *et al.* report that inhibition of the Raf/Mek/Erk pathway in the human leukaemia cell line K562 induced both growth inhibition and apoptosis [84]. The observed reduction in viability following inhibition of $cPLA_2\alpha$ in CCRF-CEM might therefore be a result of reduced levels of PGE_2.

LTB_4 promotes proliferation and cell survival through the Mek/Erk and PI3K/Akt pathways (Figure 5.1). Deregulation of the PI3K pathway has been found in numerous malignancies, including lymphoid cancer [85]. Activating phosphorylation of Akt by PI3K allows Akt to further phosphorylate several components of the cell death machinery, and thereby prevent apop-

tosis. In addition to inhibit apoptosis, Akt promote cell survival by phosphorylation and activation of IκB kinase (IKK). IKK induce degradation of the nuclear factor κB (NF-κB) inhibitor, and as a consequence allow the release of transcription factor NF-κB from the cytoplasm. NF-κB is essential in the activation of genes involved in cell survival, and with no inhibitory signal present, it can freely translocate to the nucleus and stimulate cell survival [85].

Downstream products of cPLA$_2$α are likely to contribute to cancer progression through multiple signal pathways, identifying cPLA$_2$α as a potential therapeutic target to reduce cancer progression. To unravel the specific mechanisms at play, further investigations are needed.

5.7 Serum effects

When assessing the cells' viability with resazurin, the serum concentration was shown to affect viability, regardless of the inhibitors. For Compound 2, the IC50 values were significantly lower in medium supplemented with 10% FBS, whereas for BKM120, the IC50 values were slightly lower in serum deprived medium. It was not possible to determine IC50 values for Compounds 1 and 3 in medium supplemented with 10% FBS, suggesting that factors present in the added serum interacted with the inhibitors and prevents Compounds 1 and 3 from interacting with the cells.

A serum effect was also present in the analyses of cell death after treatment with BKM120. The inhibitor was tested in medium supplemented with both 10% and 0.5% FBS. Here, we found that in serum deprived medium, the inhibitor displayed a preferential activation of apoptosis. This trend was not observed in medium supplemented with 10% FBS, in which the apoptotic and necrotic populations were of the same sizes for all the tested doses of BKM120. As the serum concentration was the only altered experimental parameter, the contrasting response to the inhibitor can be asigned to the serum concentration. Interestingly, this finding suggests that the serum has a protective effect.

Preliminary experiments to determine the ideal seeding density in 96 well plates and resazurin incubation time were only conducted in medium supplemented with 10% FBS (Appendix B). As the serum concentration has proven to affect several of the measured parameters, such preliminary experiments should also have been conducted in serum deprived medium. This would not only have allowed for the optimisation of experimental conditions with 10% FBS, but also with serum deprivation.

5.8 The significance of statistical analyses

As a rule of thumb, statistical analyses are performed on data sets to identify significant differences between controls and various treatments. In this thesis, most of the experiments were repeated several times with multiple biological and technical replicates. By doing so, random biological variations and technical errors are represented in the standard deviation (SD) of the mean. When determining significance, consideration is given to the SD of each of the means, allowing an accurate determination of treatment effect.

When investigating the statistical significance between treatments, is is important to make sure that the data set meets the requirements for the selected statistical analysis. Generally, one-way ANOVA is used to establish significance between treatment groups and a control. One of the requirements for ANOVA is equal variance between groups [86]. To test whether this requirement was met, QQ plots with predicted residuals were made (data not shown). The residuals were not located along the diagonal line, indicating that the requirement of equal variance was not met and the normal one-way ANOVA could therefore not be used. To circumvent the issue with unequal variance, the Welch's ANOVA was used instead, as this does not require equal variance. Furthermore, when comparing multiple treatments to the same control, the rate of type 1 error increases. It was therefore necessary to perform post hoc tests to correct the p-values generated by Welch's ANOVA. Due to unequal variance between treatments, as well as variations in group sizes, Tamhane T2 correction for multiple comparisons

was used [87].

The importance of statistical analyses became evident when synergy was determined after measurements of viability with the resazurin assay. The calculations of CIs by Bliss Independence did not consider the SD from the relative reduction in viability after treatment with inhibitors. As a result, the CIs alone indicated synergy, whereas Welch's ANOVA with Tamhane T2 correction for multiple comparisons suggested the opposite. In this case, the Welch's ANOVA with corrections included factors such as group size and variance which were ignored by Bliss Independence. The statistical analyses were therefore considered more reliable than the CI value, taking additional parameters into account and giving a more balanced value. If the statistics were wrongly used or not considered properly, it would have resulted in a false conclusion of synergy. As such, this example demonstrated the importance of putting the significance of statistical analyses in focus.

6 Future perspectives

Cancer is one of the biggest mysteries in medicine today, and there is an ongoing battle to unravel the underlying mechanisms of cancer progression and identify factors that are essential for the cancer to survive and thrive. Cancers have shown to be dependent on pathways regulated by Ras and TNF, and it would be of great interest to investigate how inhibition of cPLA$_2\alpha$ would affect other types of cancer displaying an upregulation of Ras and insensitivity for apoptosis induced by TNF. By inducing cell death through the novel inhibition of cPLA$_2\alpha$, resistance to several chemotherapies might be avoided, and thus improve treatment of numerous cancers.

As a continuation of the investigation of the role of cPLA$_2\alpha$ in T-ALL, the experiments investigating mode of death in different serum concentrations should be optimised and repeated. Furthermore, the eicosanoid levels in the cells following inhibition of cPLA$_2\alpha$ should be quantified to verify that the reduction in viability is a result of reduced eicosanoid concentrations.

Since eicosanoids act in a paracrine manner, the specific inhibition of cPLA$_2\alpha$ in cancer cells might also affect the tumour microenvironment. There is still much to learn about the interactions that occur in the tumour microenvironment, but there are reasons to believe that lipid mediators derived from arachidonic acid play a vital part in this complex communication. By removing drivers of proliferation and cell survival, cancer progression can efficiently be slowed down and potentially completely stopped. Therefore, inhibition of cPLA$_2\alpha$ will not only reduce the viability amongst cancer cells, but it will also make the tumour microenvironment less cancer friendly. To establish the role of cPLA$_2\alpha$ in the tumour microenvironment of T-ALL, it would be extremely interesting and valuable if the research could continue in a suitable animal model. Several of the inhibitors developed by Avexxin have been proven efficient in mouse models, suggesting that mice with T-ALL would pose as fitting models to establish the role of cPLA$_2\alpha$ in the tumour microenvironment.

References

1. *Cancer* Oxford Dictionaries. `https://en.oxforddictionaries.com` (2019).
2. Ames, B. N., Gold, L. S. & Willett, W. C. The causes and prevention of cancer. *Proceedings of the National Academy of Sciences of the United States of America* **92,** 5258–65 (1995).
3. Griffiths, A. J., Miller, J. H., Suzuki, D. T., Lewontin, R. C. & Gelbart, W. M. *Mutation and cancer* in *An introduction to Genetic Analysis* 7th ed. (W. H. Freeman, 2000).
4. Levine, A. J. The tumor suppressor genes. *Annual Review of Biochemistry* **62,** 623–651 (1993).
5. Hussain, S. P. & Harris, C. C. Molecular epidemiology of human cancer: contribution of mutation spectra studies of tumor suppressor genes. *Cancer research* **58,** 4023–37 (1998).
6. Canman, C. E. & Kastan, M. B. Induction of apoptosis by tumor suppressor genes and oncogenes. *Seminars in Cancer Biology* **6,** 17–25 (1995).
7. Harrington, E. A., Fanidi, A. & Evan, G. I. Oncogenes and cell death. *Current Opinion in Genetics & Development* **4,** 120–129 (1994).
8. Roomi, W. M., Neha, S., Niedzwiecki, A. & Rath, M. Vitamin C in Health: Scientific focus on its anti-cancer efficacy. *Journal of Cellular Medicine and Natural Health* (2015).
9. Alberts, B. *et al. Molecular biology of the cell* in *Molecular biology of the cell* 6th ed. (Garland Science, New York, 2015).
10. Wang, M. *et al.* Role of tumor microenvironment in tumorigenesis. *Journal of Cancer* **8,** 761–773 (2017).
11. Cooper, G. M. *15. Cancer* in *The cell. A molecular Approach* 2nd ed. (Sinauer Associates, Sunderland, 2000).
12. Visvader, J. E. Cells of origin in cancer. *Nature* **469,** 314–322 (2011).
13. Gerber, H.-P. & Ferrara, N. The role of VEGF in normal and neoplastic hematopoiesis. *Journal of Molecular Medicine* **81,** 20–31 (2003).

14. Kondo, M. Lymphoid and myeloid lineage commitment in multipotent hematopoietic progenitors. *Immunological reviews* **238,** 37–46 (2010).
15. Olsson, I., Bergh, G., Ehinger, M. & Gullberg, U. Cell differentiation in acute myeloid leukemia. *European journal of haematology* **57,** 1–16 (1996).
16. Murphy, K. & Weaver, C. *Janeway's Immunobiology* in *Janeway's Immunobiology* (eds Toledo, M., Bochicchio, A., Acevedo-Quiñones, C., Zayetz, E. & Divakaran, D.) 9th ed. (Garland Science, New York, 2017).
17. Owen, J., Punt, J. & Stanford, S. A. *2. Cells, Organs, and Microenvironments of the Immune System* in *Kuby immunology* (eds Punt, J., Stranford, S. A. & Jones, P. P.) 7th ed. (Freeman, New York, 2013).
18. Häggström, M. & Rad, A. *Simplified haematopoiesis* `https://en.wikipedia.org/wiki/Haematopoiesis#/media/File:Hematopoiesis_simple.svg`.
19. Rabbitts, T. H. Translocations, master genes, and differences between the origins of acute and chronic leukemias. *Cell* **67,** 641–644 (1991).
20. Shapira, T., Pereg, D. & Lishner, M. How I treat acute and chronic leukemia in pregnancy. *Blood Reviews* **22,** 247–259 (2008).
21. McKew, S., Rajab, J. & Bates, I. *Hematologic Diseases* in *Hunter's Tropical Medicine and Emerging Infectious Disease* 35–46 (W.B. Saunders, 2013).
22. Redaelli, A., Laskin, B. L., Stephens, J. M., Botteman, M. F. & Pashos, C. L. A systematic literature review of the clinical and epidemiological burden of acute lymphoblastic leukaemia (ALL). *European Journal of Cancer Care* **14,** 53–62 (2005).
23. Ah-Moye, D., Davies, C., Goody, J., Hayward, P. & Frewin, R. Introduction to haematology and transfusion science. *Clinical Biochemistry: Metabolic and Clinical Aspects,* 497–514 (2014).
24. Shah, N. N. & Wayne, A. S. *Acute Lymphoblastic Leukemia* in *The Bethesda Handbook of Hematology* 3rd ed. (Lippincott Williams & Wilkins, Philadelphia, 2013).

25. Terwilliger, T. & Abdul-Hay, M. Acute lymphoblastic leukemia: a comprehensive review and 2017 update. *Blood Cancer Journal* **7,** e577 (2017).
26. Hunger, S. P. & Mullighan, C. G. Acute Lymphoblastic Leukemia in Children. *New England Journal of Medicine* **373,** 1541–1552 (2015).
27. Hoelzer, D. Personalized medicine in adult acute lymphoblastic leukemia. *Haematologica* **100,** 855–858 (2015).
28. Roberts, K. G. & Mullighan, C. G. Genomics in acute lymphoblastic leukaemia: insights and treatment implications. *Nature Reviews Clinical Oncology* **12,** 344–357 (2015).
29. Foley, G. E. *et al.* Continuous culture of human lymphoblasts from peripheral blood of a child with acute leukemia. *Cancer* **18,** 522–529 (1965).
30. Lambrou, G. *et al.* Pathway simulations in common oncogenic drivers of leukemic and rhabdomyosarcoma cells: A systems biology approach. *International journal of oncology* **40,** 1365–1390 (2012).
31. Cooper, G. M. *14. The Eukaryotic Cell Cycle* in *The cell. A molecular Approach* 2nd ed. (Sinauer Associates, Sunderland, 2000).
32. Alberts, B. *et al. Molecular biology of the cell* in *Molecular biology of the cell* 6th ed. (Garland Science, New York, 2015).
33. Galluzzi, L. *et al.* Molecular mechanisms of cell death: recommendations of the Nomenclature Committee on Cell Death 2018. *Cell Death & Differentiation* **25,** 486–541 (2018).
34. Apraiz, A., Boyano, M. D. & Asumendi, A. Cell-Centric View of Apoptosis and Apoptotic Cell Death-Inducing Antitumoral Strategies. *Cancers* **3,** 1042–1080 (2011).
35. Henry, C. M., Hollville, E. & Martin, S. J. Measuring apoptosis by microscopy and flow cytometry. *Methods* **61,** 90–97 (2013).
36. Murphy, K. & Weaver, C. *Janeway's Immunobiology* in *Janeway's Immunobiology* (eds Toledo, M., Bochicchio, A., Acevedo-Quiñones, C., Zayetz, E. & Divakaran, D.) 9th ed. (Garland Science, New York, 2017).

37. Sckisel, G. D. *et al.* English. *Impact of ageing and body mass on cancer immunotherapy outcomes* in *Tumor Immunology and Immunotherapy* (ed Rees, R. C.) (Oxford University Press, Oxford, UK, 2014).
38. Kennedy, S. R., Loeb, L. A. & Herr, A. J. Somatic mutations in aging, cancer and neurodegeneration. *Mechanisms of Ageing and Development* **133,** 118–126 (2012).
39. Qi, H.-Y. *et al.* A cytosolic phospholipase A_2 ($cPLA_2$)-initiated lipid mediator pathway induces autophagy in macrophages. *Journal of immunology* **187,** 5286–5292 (2011).
40. Sun, G. Y. *et al.* Phospholipases A2 and inflammatory responses in the central nervous system. *Neuromolecular medicine* **12,** 133–148 (2010).
41. Niknami, M., Patel, M., Witting, P. K. & Dong, Q. Molecules in focus: Cytosolic phospholipase $A_2-\alpha$. *The International Journal of Biochemistry & Cell Biology* **41,** 994–997 (2009).
42. Burke, J. E. & Dennis, E. A. Phospholipase A_2 Biochemistry. *Cardiovascular Drugs and Therapy* **23,** 49–59 (2009).
43. Kramer, R. M. & Sharp, J. D. Structure, function and regulation of Ca^2+-sensitive cytosolic phospholipase A2 ($cPLA_2$). *FEBS Letters* **410,** 49–53 (1997).
44. Burke, J. E. & Dennis, E. A. Phospholipase A2 structure/function, mechanism, and signaling. *Journal of lipid research* **50 Suppl,** S237–42 (2009).
45. Haeggström, J. Z., Rinaldo-Matthis, A., Wheelock, C. E. & Wetterholm, A. Advances in eicosanoid research, novel therapeutic implications. *Biochemical and Biophysical Research Communications* **396,** 135–139 (2010).
46. Dessen, A. *et al.* Crystal Structure of Human Cytosolic Phospholipase A2 Reveals a Novel Topology and Catalytic Mechanism. *Cell* **97,** 349–360 (1999).
47. Harizi, H., Corcuff, J.-B. & Gualde, N. Arachidonic-acid-derived eicosanoids: roles in biology and immunopathology. *Trends in Molecular Medicine* **14,** 461–469 (2008).

48. Balkwill, F. & Mantovani, A. Inflammation and cancer: back to Virchow? *The Lancet* **357,** 539–545 (2001).
49. Coussens, L. M. & Werb, Z. Inflammation and cancer. eng. *Nature* **420,** 860–867 (2002).
50. Grivennikov, S. I., Greten, F. R. & Karin, M. Immunity, Inflammation, and Cancer. *Cell* **140,** 883–899 (2010).
51. Mantovani, A. Molecular pathways linking inflammation and cancer. *Current molecular medicine* **10,** 369–73 (2010).
52. Bennett, M. & Gilroy, D. W. Lipid Mediators in Inflammation. *Microbiology Spectrum* **4** (2016).
53. Wang, D. & Dubois, R. N. Eicosanoids and cancer. *Nature reviews. Cancer* **10,** 181–93 (2010).
54. *CCRF-CEM (ATCC CCL-119)* ATCC. `https://www.lgcstandards-atcc.org/products/all/CCL-119.aspx?geo_country=no#culturemethod` (2019).
55. Uzbekov, R. E. Analysis of the Cell Cycle and a Method Employing Synchronized Cells for Study of Protein Expression at Various Stages of the Cell Cycle. *Biochemistry (Moscow)* **69,** 485–496 (2004).
56. Vega-Avila, E. & Pugsley, M. K. An overview of colorimetric assay methods used to assess survival or proliferation of mammalian cells. *Proceedings of the Western Pharmacology Society* **54,** 10–14 (2011).
57. O'Brien, J., Wilson, I., Orton, T. & Pognan, F. Investigation of the Alamar Blue (resazurin) fluorescent dye for the assessment of mammalian cell cytotoxicity. *European Journal of Biochemistry* **267,** 5421–5426 (2000).
58. Chabner, B. A. & Roberts Jr, T. G. Chemotherapy and the war on cancer. *Nature Reviews Cancer* **5,** 65 (2005).
59. Gottesman, M. M. Mechanisms of Cancer Drug Resistance. *Annual Review of Medicine* **53,** 615–627 (2002).
60. Foucquier, J. & Guedj, M. Analysis of drug combinations: current methodological landscape. *Pharmacology research & perspectives* **3** (2015).
61. Shapiro, H. M. Multistation multiparameter flow cytometry: A critical review and rationale. *Cytometry* **3,** 227–243 (1983).

62. Adan, A., Alizada, G., Kiraz, Y., Baran, Y. & Nalbant, A. Flow cytometry: basic principles and applications. *Critical Reviews in Biotechnology* **37,** 163–176 (2017).
63. Brown, M. & Wittwer, C. Flow Cytometry: Principles and Clinical Applications in Hematology. *Clinical Chemistry* **46,** 1221 LP –1229 (2000).
64. *CellEvent™ Caspase-3/7 Green Flow Cytometry Assay Kit* (ThermoFisher Scientific, 2016).
65. *SYTOX AADvanced™ Dead Cell Stain Kits* (ThermoFisher Scientific, 2008).
66. Nunez, R. DNA Measurement and Cell Cycle Analysis by Flow Cytometry. *Current issues in molecular biology* **3,** 67–70 (2001).
67. Navas, P. *et al.* Ceramide-dependent Caspase 3 Activation is Prevented by Coenzyme Q from Plasma Membrane in Serum-deprived Cells. *Free Radical Research* **36,** 369–374 (2002).
68. Wu, Y., Jiang, X.-R., Newland, A. & M Kelsey, S. Failure to activate cytosolic phospholipase A2 causes TNF resistance in human leukemic cells. *Journal of immunology* **160,** 5929–5935 (1998).
69. Savva, C. G., Totokotsopoulos, S., Nicolaou, K. C., Neophytou, C. M. & Constantinou, A. I. Selective activation of TNFR1 and NF-κB inhibition by a novel biyouyanagin analogue promotes apoptosis in acute leukemia cells. *BMC Cancer* **16,** 279 (2016).
70. Cedergreen, N. Quantifying Synergy: A Systematic Review of Mixture Toxicity Studies within Environmental Toxicology. *PLoS ONE* **9,** e96580 (2014).
71. Chou, T.-C. Drug Combination Studies and Their Synergy Quantification Using the Chou-Talalay Method. *Cancer Research* **70,** 440 LP –446 (2010).
72. Lee, J. J., Kong, M., Ayers, G. D. & Lotan, R. Interaction Index and Different Methods for Determining Drug Interaction in Combination Therapy. *Journal of Biopharmaceutical Statistics* **17,** 461–480 (2007).
73. Mannello, F. & Tonti, G. A. Concise Review: No Breakthroughs for Human Mesenchymal and Embryonic Stem Cell Culture: Conditioned

Medium, Feeder Layer, or Feeder-Free; Medium with Fetal Calf Serum, Human Serum, or Enriched Plasma; Serum-Free, Serum Replacement Nonconditioned Medium, or Ad Hoc Formula? All That Glitters Is Not Gold! *Stem Cells* **25,** 1603–1609 (2007).

74. Kume, T. *et al.* Serofendic acid, a neuroprotective substance derived from fetal calf serum, inhibits mitochondrial membrane depolarization and caspase-3 activation. *European Journal of Pharmacology* **542,** 69–76 (2006).
75. Engin, A. B. *What Is Lipotoxicity?* in *Obesity and Lipotoxicity* (eds Engin, A. B. & Engin, A.) 197–220 (Springer International Publishing, 2017).
76. Muckova, K., Duffield, J. S., Held, K. D., Bonventre, J. V. & Sheridan, A. M. $cPLA_2$ -interacting protein, PLIP, causes apoptosis and decrease G1 phase in mesangial cells. *American Journal of Physiology-Renal Physiology* **290,** F70–F79 (2006).
77. Naini, S. M. *et al.* Cytosolic phospholipase $A_2\alpha$ regulates G_1 progression through modulating FOXO1 activity. *The FASEB Journal* **30,** 1155–1170 (2015).
78. Movahedi Naini, S., Sheridan, A. M., Force, T., Shah, J. V. & Bonventre, J. V. Group IVA Cytosolic Phospholipase A_2 Regulated the G_2-to-M Transition by Modulating the Activity of Tumor Suppressor SIRT2. *Molecular and Cellular Biology* **35,** 3768 LP –3784 (2016).
79. Khan, K. H., Yap, T. A., Yan, L. & Cunningham, D. Targeting the PI3K-AKT-mTOR signaling network in cancer. *Chinese journal of cancer* **32,** 253–65 (2013).
80. Giancotti, F. G. Deregulation of Cell Signaling in Cancer. *FEBS letters* **588,** 2558 (2014).
81. Park, J. B. *et al.* Phospholipase signalling networks in cancer. *Nature Reviews Cancer* **12,** 782–792 (2012).
82. Moharram, S. A., Shah, K. & Kazi, J. U. T-cell Acute Lymphoblastic Leukemia Cells Display Activation of Different Survival Pathways. *Journal of Cancer* **8,** 4124 (2017).

83. Jancík, S., Drábek, J., Radzioch, D. & Hajdúch, M. Clinical relevance of KRAS in human cancers. *Journal of biomedicine & biotechnology* **2010,** 150960 (2010).
84. Chan, K. T. *et al.* Cucurbitacin B inhibits STAT3 and the Raf/MEK/ERK pathway in leukemia cell line K562. *Cancer Letters* **289,** 46–52 (2010).
85. Vivanco, I. & Sawyers, C. L. The phosphatidylinositol 3-Kinase–AKT pathway in human cancer. *Nature Reviews Cancer* **2,** 489–501 (2002).
86. Løvås, G. G. *8. Sammenlikning av grupper* in *Statistikk for universiteter og høgskoler* 3rd ed., 340–350 (Universitetsforlaget, 2013).
87. Shingala, M. C. & Rajyaguru, A. *International Journal of New Technologies in Science and Engineering* **2** (5 2015).

Appendix A Reagents

Table A.1 presents the mode of action and target of the compounds used in this work. General equipment and reagents used are given in Table A.2.

Table A.1: Mode of action and targets for the five inhibitors used.

Compound	Mode of action	Target
BKM120	Inhibitory	PI3 kinase
Compound 1	Inhibitory	cPLA$_2\alpha$
Compound 2	Inhibitory	cPLA$_2\alpha$
Compound 3	Inhibitory	cPLA$_2\alpha$
Compound 4	Inhibitory	cPLA$_2\alpha$

Table A.2: List of general equipment and reagents used, the vendor from which they were acquired and the corresponding catalogue number.

Reagent	Vendor	Catalogue no.
Cell cultivation		
RPMI-1640 Medium	Sigma-Aldrich	R0883
Foetal bovine serum	Gibco	10270
		LOT 41Q9248K
L-Glutamine	Lonza	17-605E/12
Gentamicin	Sigma-Aldrich	G1397
Trypan Blue	Sigma-Aldrich	T8154-100ML
Corning 75 cm^2 Cell culture flask	Sigma-Aldrich	CLS430641U
Resazurin assay		
Resazurin	RD Systems	AR002
		LOT 1470147
Cell death assay		
CellEvent™ Caspase-3/7 Green Flow Cytometry Assay Kit	Thermo Fisher Scientific	C10427
Cell cycle arrest		
Propidium iodide	Sigma-Aldrich	81845-100MG
RNase	Sigma-Aldrich	R6513-10MG
Methanol	VWR	24229-2.5L

Appendix B Preliminary experiments

B.1 Seeding density

Cells were seeded in 96 well plates at four different densities to determine the ideal seeding density in experiments, as shown in Figure B.1. Based on the low SD, the optimal seeding density in 96 well plates was determined to be 50 000 cells/well.

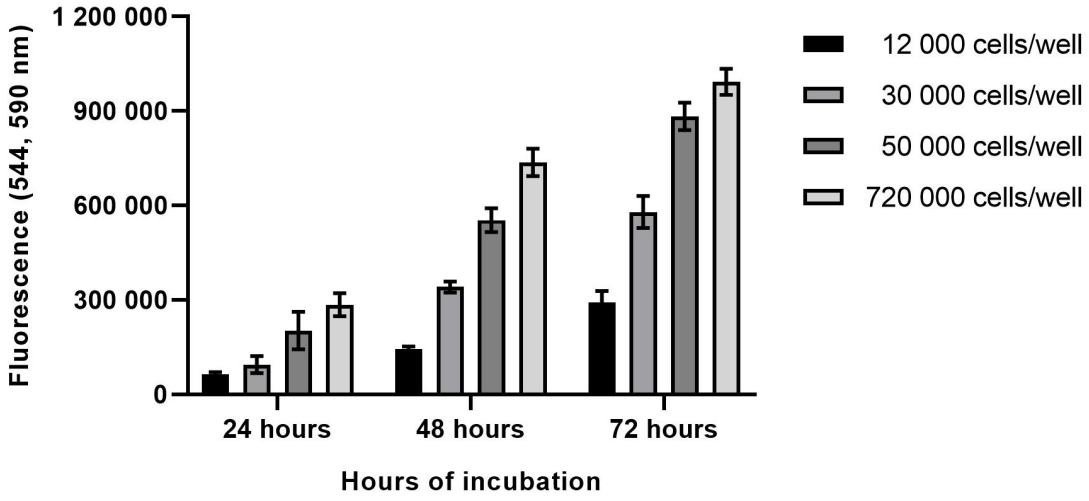

Figure B.1: Four cell densities were seeded in 96 well plates and incubated for 24, 48 and 72 hours in complete growth medium supplemented with 10% FBS. The cells were analysed using resazurin assay and measured by fluorescence.

B.2 Resazurin incubation time

The incubation time with resazurin was investigated in cells seeded at an initial density of 50 000 cells/well. Cells were grown for 24, 48 and 72 hours, before the relative fluorescence was measured after incubation with resazurin for 1, 2, 3 and 4 hours. The mean fluorescence of six technical replicates ± SD is presented in Figure B.2. Cells incubated with resazurin for 2 and 3 hours displayed the lowest SD for all three time points, and thus considered the best incubation period. An incubation period of 2 hours was chosen for convenience.

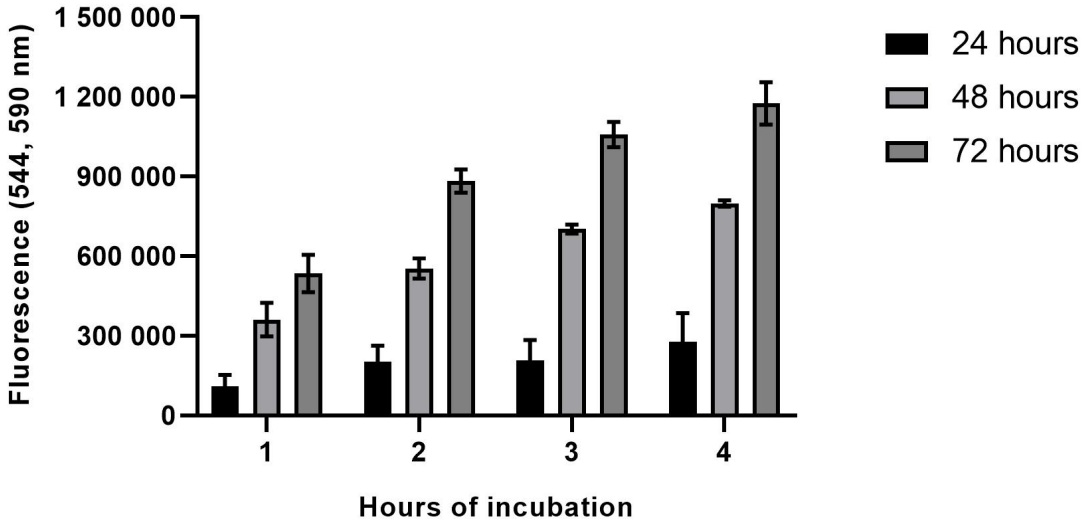

Figure B.2: Cells seeded at an initial density of 50 000 cells/well and grown for 72 hours. Fluorescence were measured every 24 hours, after incubation with resazurin for 1, 2, 3 and 4 hours. Fluorescence is given as the mean of six technical replicates ± SD.

B.3 Culture medium

The effects of DMSO was investigated to find the optimal concentration which allow for the inhibitors to be fully dissolved in the serum, without the DMSO affecting cell viability. Cells treated with medium without addition of DMSO were set to 100% relative viability as a control. Table B.1 indicate that cell viability was not significantly affected in cells treated with less than 1% DMSO in either CGM or SM.

Table B.1: Cells grown in CGM and SM supplemented with varying concentrations of DMSO. Relative viability (Rel. viability) where 0% DMSO is set to 100%. P-value based on Welch's ANOVA with Tamhane T2 correction between treatments and 0% DMSO.

	CGM		SM	
DMSO (%)	Rel. viability (%)	P-value	Rel. viability (%)	P-value
0	100	-	100	-
0.1	99	0.986	100	0.999
0.2	100	0.999	98	0.868
0.5	99	0.978	99	0.919
1	98	0.649	91	0.003

Appendix C Additional data - growth curves

The growth curves in Figure 4.1 are based on three biological replicates with passage numbers 13, 20 and 24. For each time point, three separate samples from the cell culture was counted. The average for each time point with the corresponding standard deviation is presented in Tables C.1–C.3.

Table C.1: Mean cell density (cells/mL) and SD of counted cells for the density of 25 000 cells/mL. All time points represent a mean of three technical replicates.

Time (h)	Mean rep. 1	± SD	Mean rep. 2	± SD	Mean rep. 3	± SD
12	40 067	9 351	28 933	10 229	41 567	9 211
24	36 133	16 739	28 933	9 211	36 167	2 593
48	63 800	14 274	43 367	15 942	22 967	14 265
72	159 000	2 828	72 267	16 739	66 867	5 138
96	222 333	132 263	159 000	39 908	119 333	44 97
120	654 333	108 880	305 333	6 600	339 000	18 403
144	141 6667	32 998	661 333	35 910	466 333	37748
196	2 030 000	406 530	1 170 000	14 142	1 035 000	104 464

Table C.2: Mean cell density (cells/mL) and SD of counted cells for the density of 100 000 cells/mL. All time points represent a mean of three technical replicates.

Time (h)	Mean rep. 1	± SD	Mean rep. 2	± SD	Mean rep. 3	± SD
12	117 667	5 185	106 600	44 303	122 667	24 363
24	143 000	6 683	126 333	17 745	139 333	9 286
48	289 000	42 528	264 000	14 353	231 333	2 357
72	630 667	74 968	500 333	57 621	321 000	20 833
96	1 142 333	111 045	833 333	111 296	702 667	44 289
120	2 716 667	212 968	1 560 000	80 416	1 353 333	217 460
144	3 606 667	82 192	3 120 000	107 083	2 666 667	106 562
196	3 843 333	359 104	3 283 333	410 718	3 463 333	253 815

Table C.3: Mean cell density (cells/mL) and SD of counted cells for the density of 400 000 cells/mL. All time points represent a mean of three technical replicates.

Time (h)	Mean rep. 1	± SD	Mean rep. 2	± SD	Mean rep. 3	± SD
12	374 000	38 184	364 667	35 827	359 667	91 047
24	641 333	56 841	533 333	40 343	513 000	44 030
48	1 133 333	49 216	983 667	69 428	954 667	146 793
72	2 426 667	208 859	1 923 333	367 454	1 813 333	231 132
96	3 510 000	269 815	2 733 333	134 247	3 196 667	179 320
120	3 903 333	254 209	3 673 333	276 446	3 710 000	136 382
144	3 533 333	368 088	3 153 333	119 536	3 856 667	280 040
196	3 070 000	314 431	3 080 000	110 454	3 330 000	147 648

Appendix D Additional data - dose response relations

The dose response relationship for a total of five inhibitors were investigated after 24, 48 and 72 hours of treatment, in both CGM and SM. A summary of the IC50 values for the investigated inhibitors under different conditions is given in Table D.1. The IC50 values are based on the dose response curves presented in Figures D.1–D.6.

Table D.1: IC50 values based on dose response curves displayed in Figures D.1–D.6. The cells were treated with the different inhibitors for 24, 48 and 72 hours in both medium supplemented with 10% and 0.5% FBS. NA indicate that it was impossible to fit a curve to the response after treatment with the inhibitor, and the IC50 values could not be determined..

Inhibitor	24 hours		48 hours		72 hours	
	0.5% FBS	10% FBS	0.5% FBS	10% FBS	0.5% FBS	10% FBS
Comp. 1	4.0 ± 0.4	NA	3.2 ± 0.3	NA	2.9 ± 0.3	NA
Comp. 2	7.6 ± 0.6	0.5 ± 0.1	5.5 ± 2.5	0.5 ± 0.02	0.6 ± 0.05	0.4 ± 0.01
Comp. 3	NA	NA	NA	NA	NA	NA
Comp. 4	9.2 ± 0.8	∼ 6	7.6 ± 0.9	NA	5.8 ± 0.5	NA
BKM120	∼ 18	∼ 6	0.9 ± 0.07	1.4 ± 0.05	1.0 ± 0.1	1.3 ± 0.05

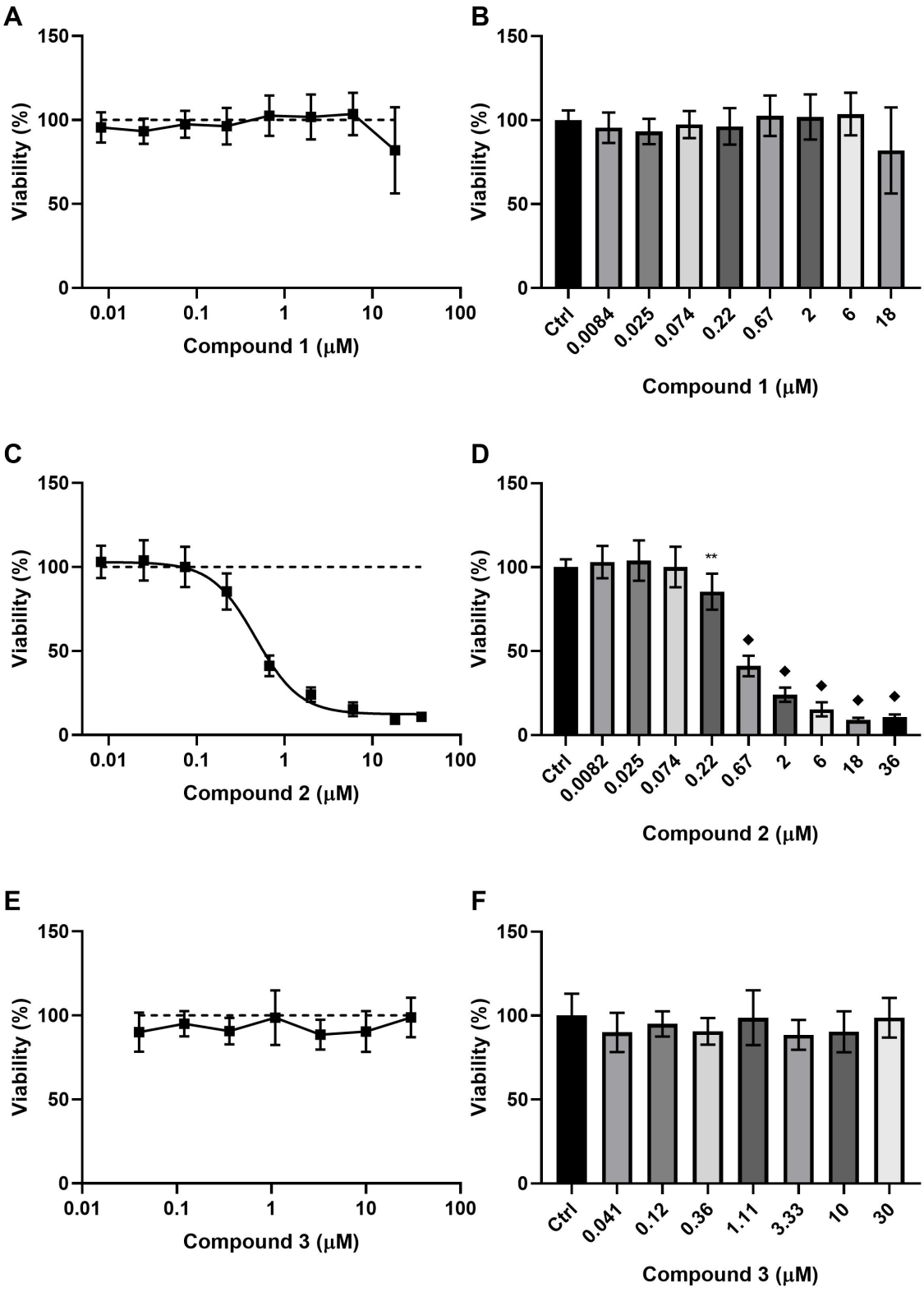
A
B
C
D
E
F
Viability (%)
150
100
50
0
0.01
0.1
1
10
100
Compound 1 (μM)
Compound 2 (μM)
Compound 3 (μM)
Ctrl
0.0084
0.025
0.074
0.22
0.67
2
6
18
0.0082
36
0.041
0.12
0.36
1.11
3.33
10
30
**

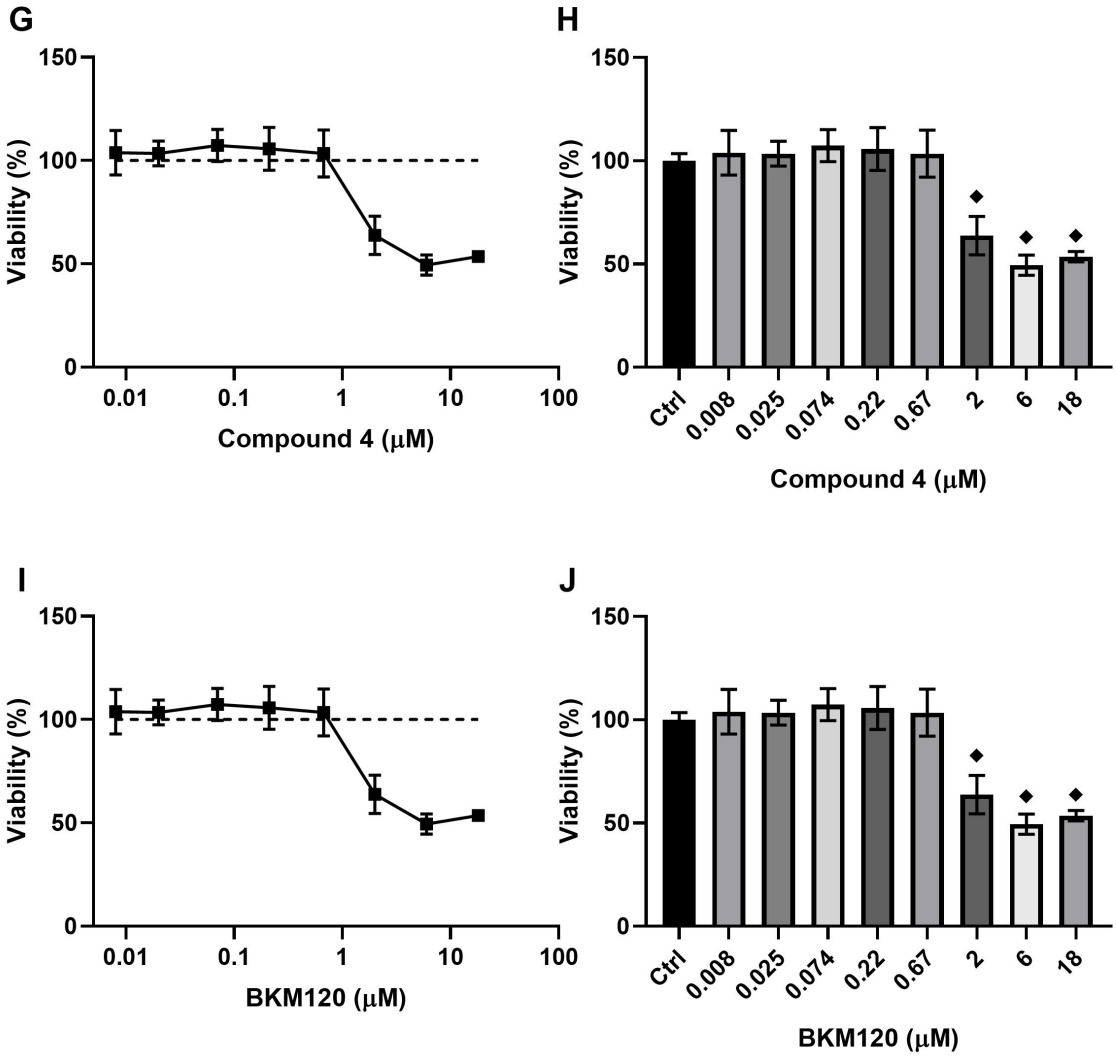

Figure D.1: Dose response correlations of selected cPLA2α inhibitors and BKM120. The dose response curves and bar graphs represent the mean relative viability ± SD across three biological replicates treated for 24 hours in CGM. The hard line represent the effects of the respective inhibitor, and the dashed line represent the control. Cells treated with 0.0082 - 18 µM of Compound 1 are shown in A and B, 0.0082 - 36 µM of Compound 2 in C and D, 0.041 - 30 µM of Compound 3 in E and F, 0.008 - 36 µM of Compound 4 in G and H and 0.0082 - 18 µM of BKM120 in I and J. Ctrl = Control treatment, set to 100% viability. * = p <0.05, ** = p <0.01, *** = p <0.001, ◆ = p <0.0001.

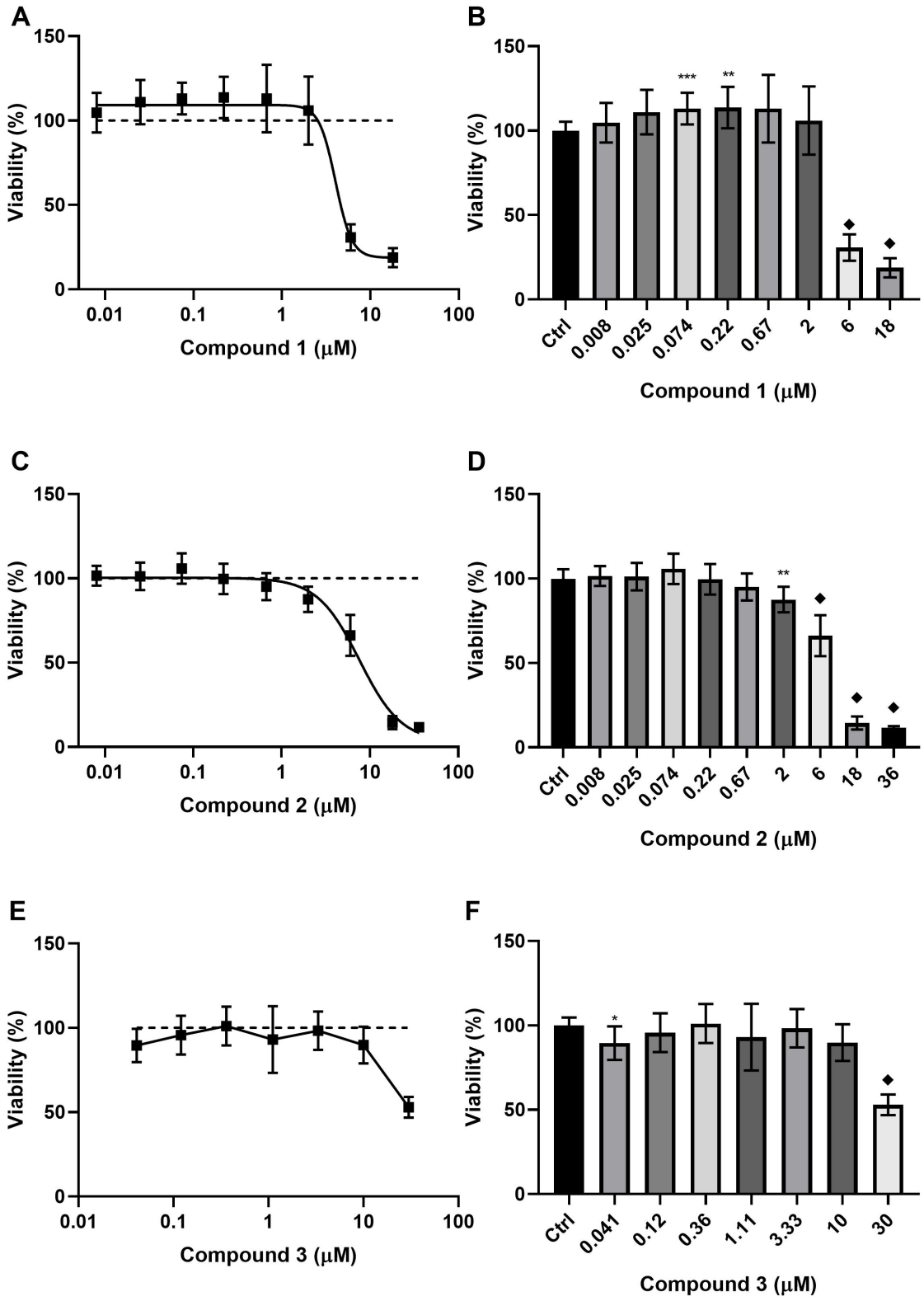
A
Viability (%)
150
100
50
0
0.01
0.1
1
10
100
Compound 1 (µM)
B
Viability (%)
***
**
Ctrl
0.008
0.025
0.074
0.22
0.67
2
6
18
Compound 1 (µM)
C
Viability (%)
Compound 2 (µM)
D
Viability (%)
**
Ctrl
0.008
0.025
0.074
0.22
0.67
2
6
18
36
Compound 2 (µM)
E
Viability (%)
Compound 3 (µM)
F
Viability (%)
*
Ctrl
0.041
0.12
0.36
1.11
3.33
10
30
Compound 3 (µM)

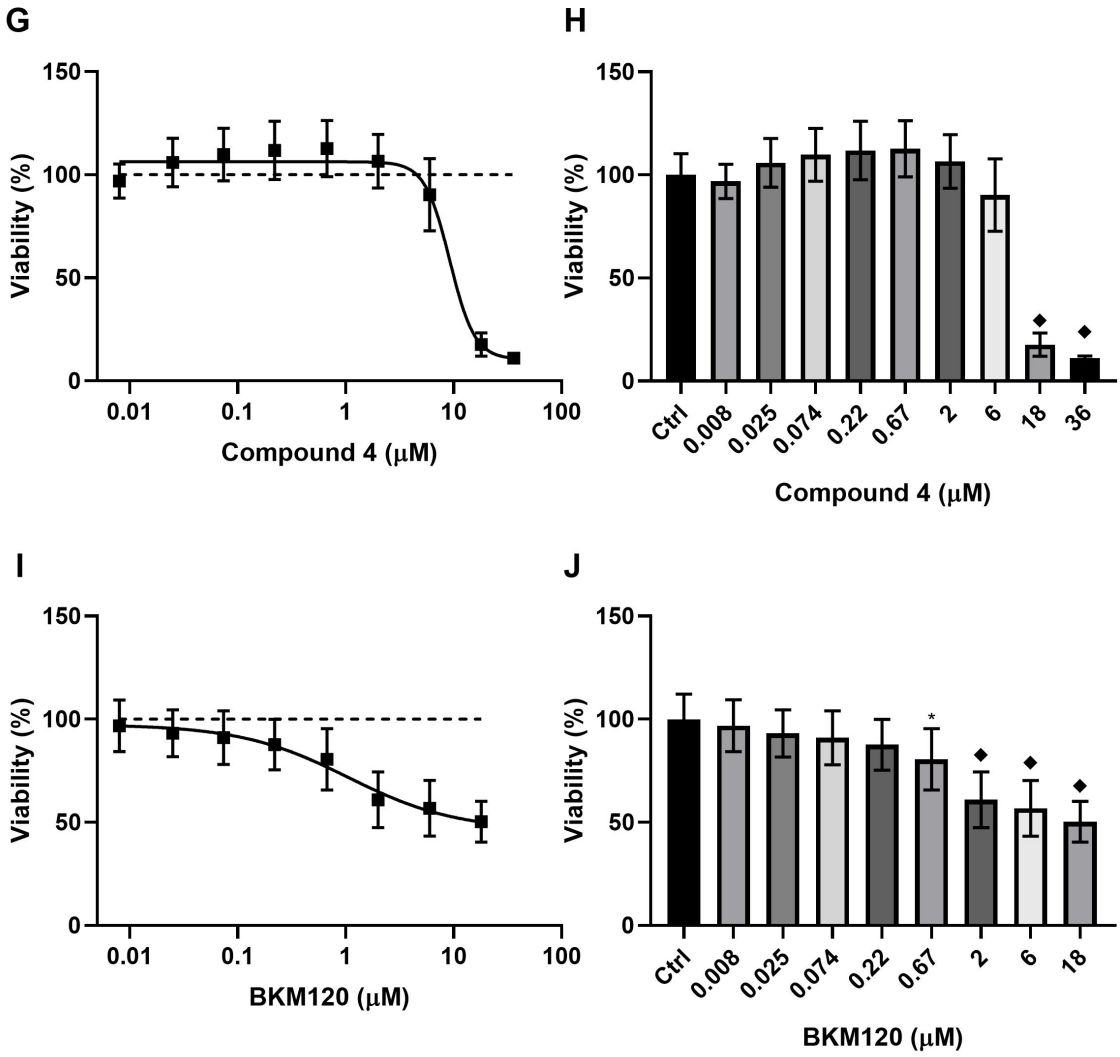

Figure D.2: Dose response correlations of selected cPLA2α inhibitors and BKM120. The dose response curves and bar graphs represent the mean relative viability ± SD across three biological replicates treated for 24 hours in SM. The hard line represent the effects of the respective inhibitor, and the dashed line represent the control. Cells treated with 0.0082 - 18 µM of Compound 1 are shown in A and B, 0.0082 - 36 µM of Compound 2 in C and D, 0.041 - 30 µM of Compound 3 in E and F, 0.008 - 36 µM of Compound 4 in G and H and 0.0082 - 18 µM of BKM120 in I and J. Ctrl = Control treatment, set to 100% viability. * = p <0.05, ** = p <0.01, *** = p <0.001, ◆ = p <0.0001.

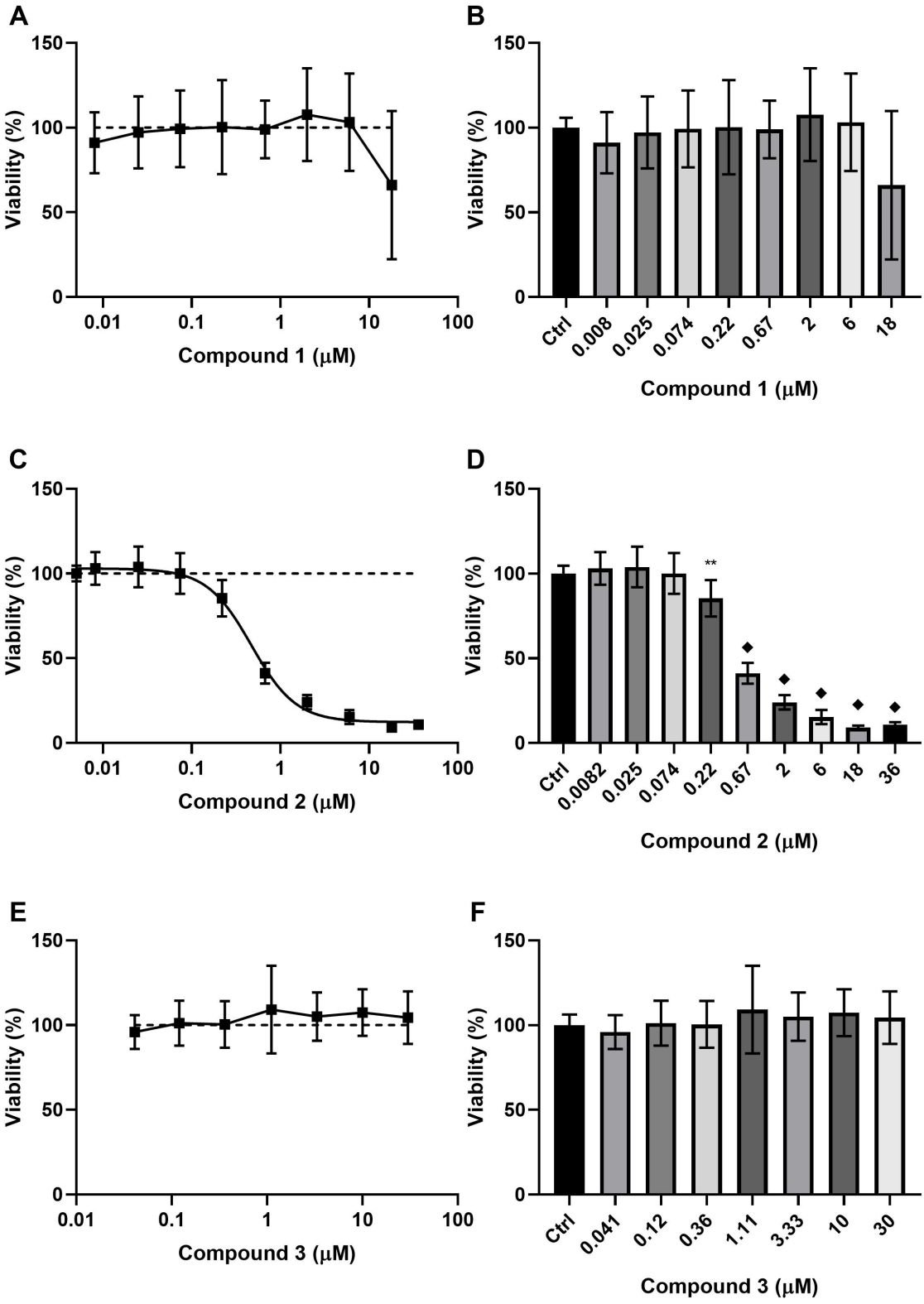
A
B
C
D
E
F
Viability (%)
150
100
50
0
0.01
0.1
1
10
100
Compound 1 (μM)
Ctrl
0.008
0.025
0.074
0.22
0.67
2
6
18
Compound 2 (μM)
0.0082
36
Compound 3 (μM)
0.041
0.12
0.36
1.11
3.33
10
30
**

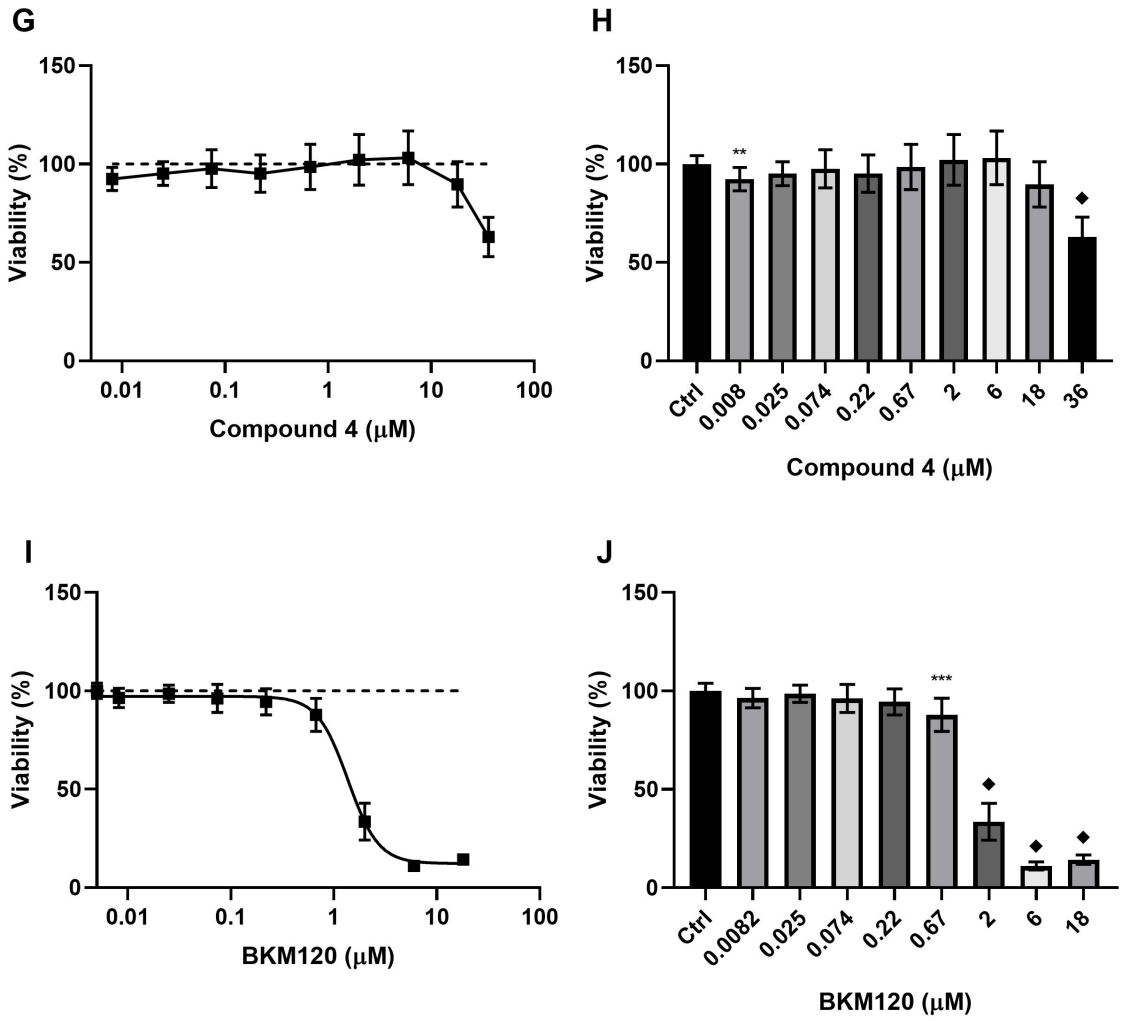

Figure D.3: Dose response correlations of selected cPLA2α inhibitors and BKM120. The dose response curves and bar graphs represent the mean relative viability ± SD across three biological replicates treated for 48 hours in CGM. The hard line represent the effects of the respective inhibitor, and the dashed line represent the control. Cells treated with 0.0082 - 18 µM of Compound 1 are shown in A and B, 0.0082 - 36 µM of Compound 2 in C and D, 0.041 - 30 µM of Compound 3 in E and F, 0.008 - 36 µM of Compound 4 in G and H and 0.0082 - 18 µM of BKM120 in I and J. Ctrl = Control treatment, set to 100% viability. * = p <0.05, ** = p <0.01, *** = p <0.001, ♦ = p <0.0001.

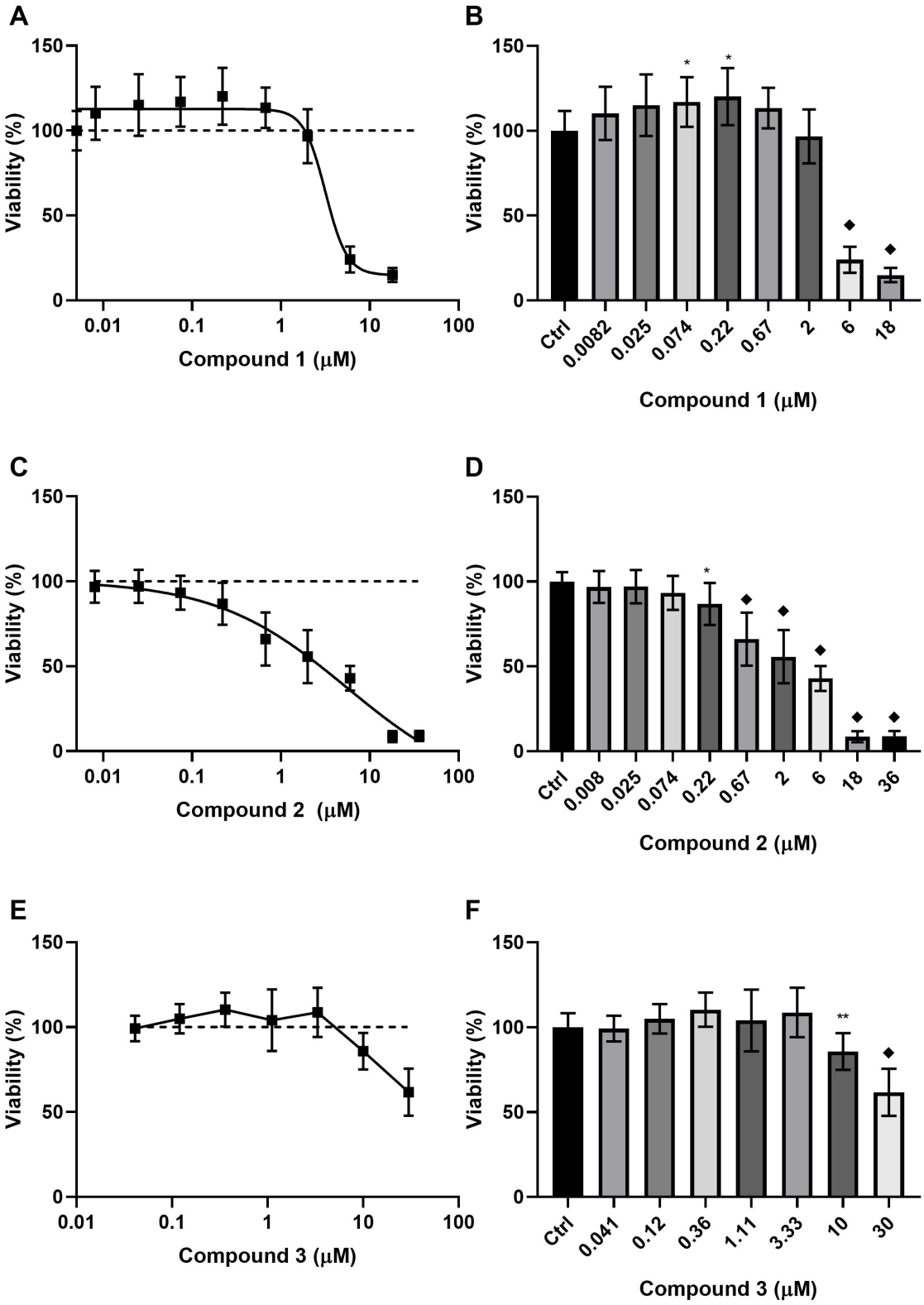
A
Viability (%)
150
100
50
0
0.01
0.1
1
10
100
Compound 1 (µM)
B
Viability (%)
150
100
50
0
*
*
◆
◆
Ctrl
0.0082
0.025
0.074
0.22
0.67
2
6
18
Compound 1 (µM)
C
Viability (%)
150
100
50
0
0.01
0.1
1
10
100
Compound 2 (µM)
D
Viability (%)
150
100
50
0
*
◆
◆
◆
◆
◆
Ctrl
0.008
0.025
0.074
0.22
0.67
2
6
18
36
Compound 2 (µM)
E
Viability (%)
150
100
50
0
0.01
0.1
1
10
100
Compound 3 (µM)
F
Viability (%)
150
100
50
0
**
◆
Ctrl
0.041
0.12
0.36
1.11
3.33
10
30
Compound 3 (µM)

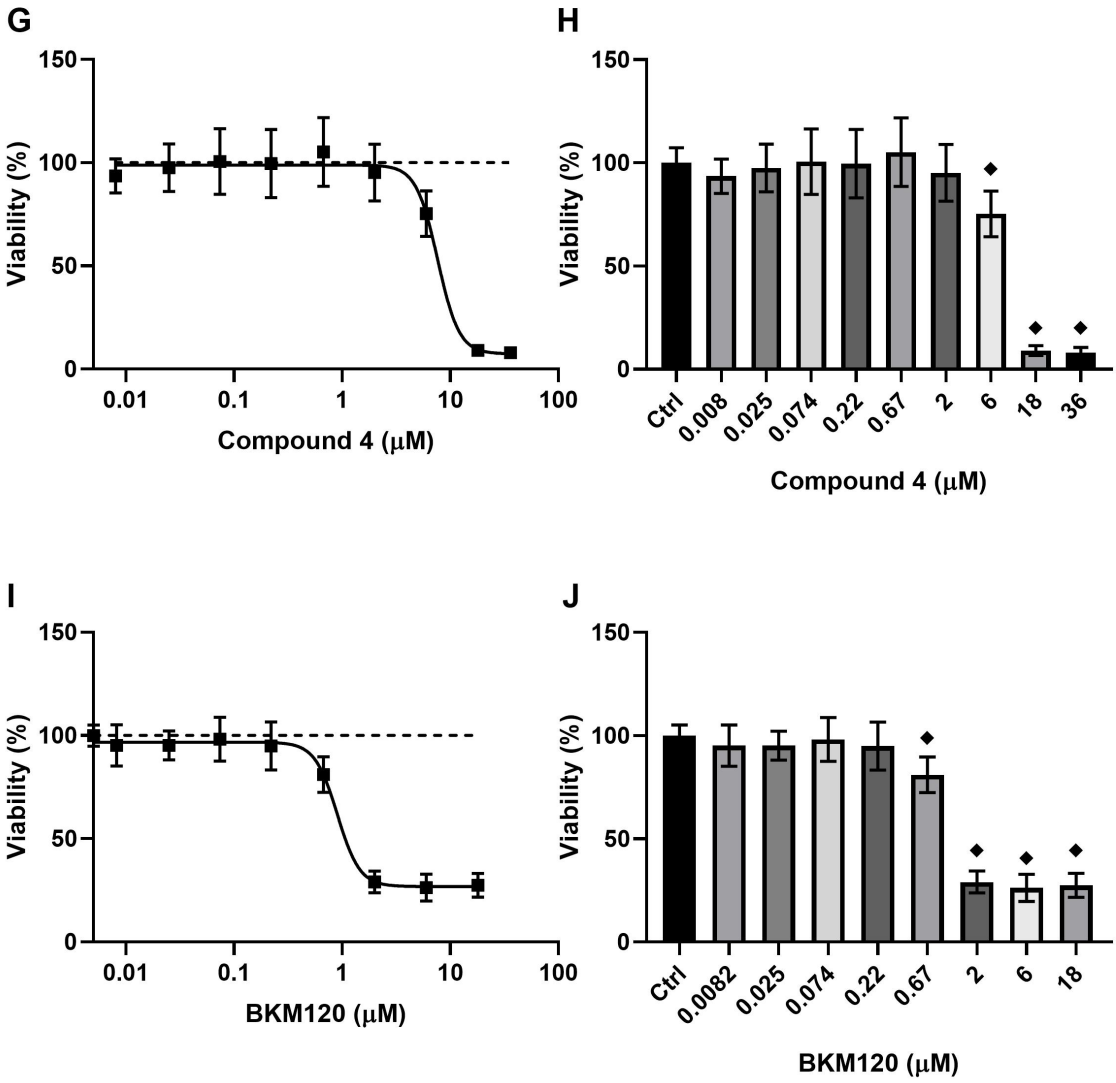

Figure D.4: Dose response correlations of selected cPLA2α inhibitors and BKM120. The dose response curves and bar graphs represent the mean relative viability ± SD across three biological replicates treated for 48 hours in SM. The hard line represent the effects of the respective inhibitor, and the dashed line represent the control. Cells treated with 0.0082 - 18 µM of Compound 1 are shown in A and B, 0.0082 - 36 µM of Compound 2 in C and D, 0.041 - 30 µM of Compound 3 in E and F, 0.008 - 36 µM of Compound 4 in G and H and 0.0082 - 18 µM of BKM120 in I and J. Ctrl = Control treatment, set to 100% viability. * = p <0.05, ** = p <0.01, *** = p <0.001, ◆ = p <0.0001.

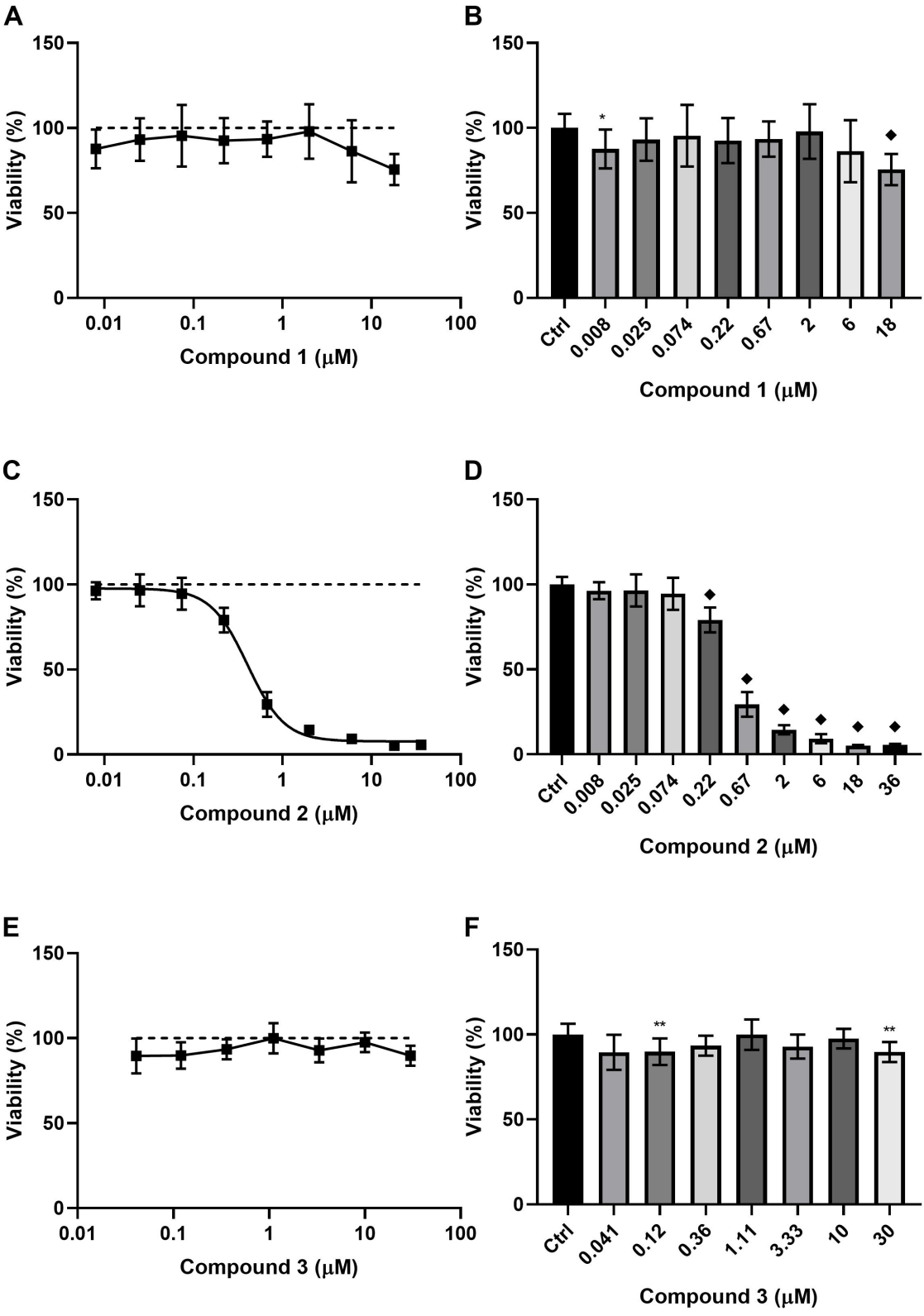
A
B
C
D
E
F
Viability (%)
150
100
50
0
0.01
0.1
1
10
100
Compound 1 (µM)
Compound 2 (µM)
Compound 3 (µM)
Ctrl
0.008
0.025
0.074
0.22
0.67
2
6
18
36
0.041
0.12
0.36
1.11
3.33
10
30
*
**

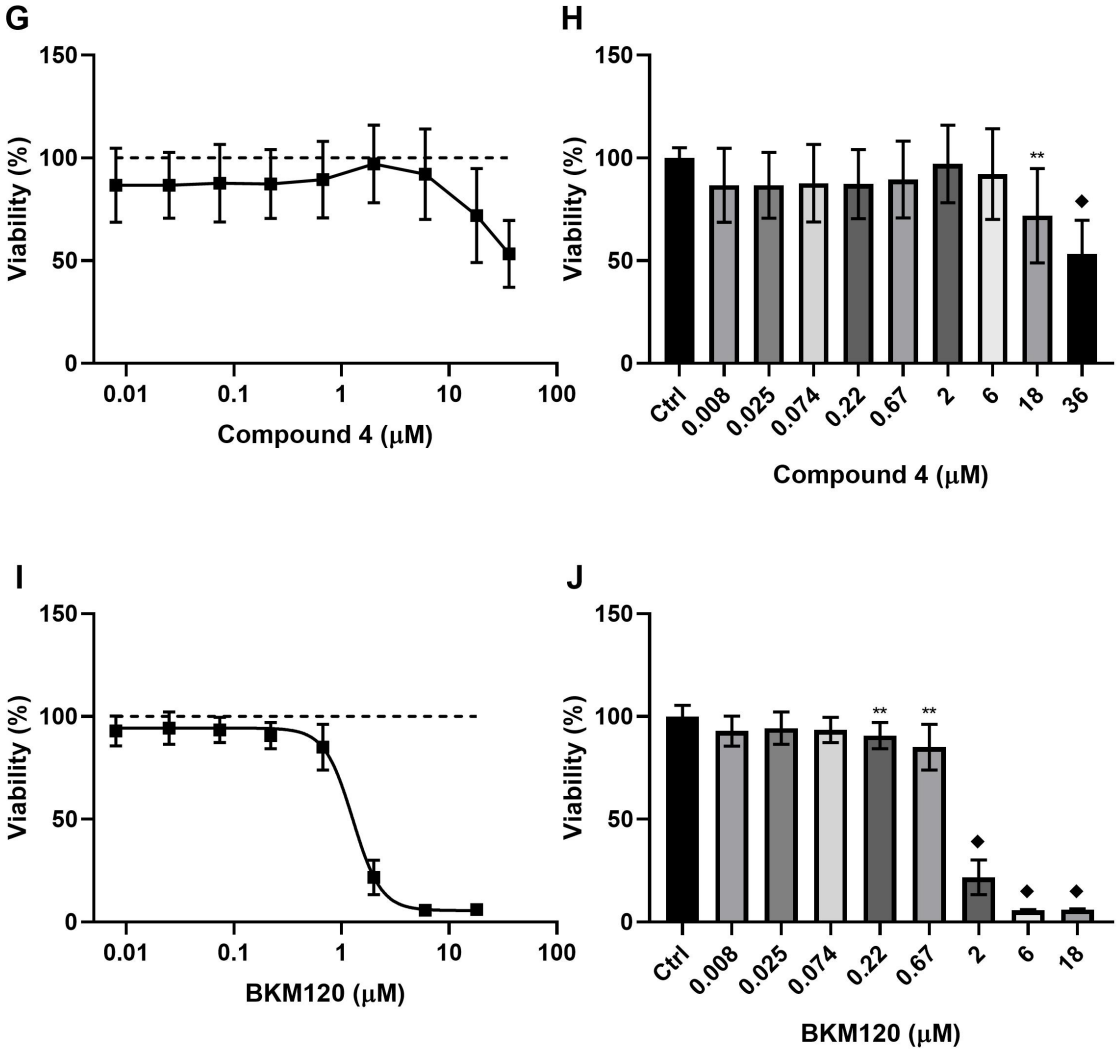

Figure D.5: Dose response correlations of selected cPLA2α inhibitors and BKM120. The dose response curves and bar graphs represent the mean relative viability ± SD across three biological replicates treated for 72 hours in CGM. The hard line represent the effects of the respective inhibitor, and the dashed line represent the control. Cells treated with 0.0082 - 18 µM of Compound 1 are shown in A and B, 0.0082 - 36 µM of Compound 2 in C and D, 0.041 - 30 µM of Compound 3 in E and F, 0.008 - 36 µM of Compound 4 in G and H and 0.0082 - 18 µM of BKM120 in I and J. Ctrl = Control treatment, set to 100% viability. * = p <0.05, ** = p <0.01, *** = p <0.001, ◆ = p <0.0001.

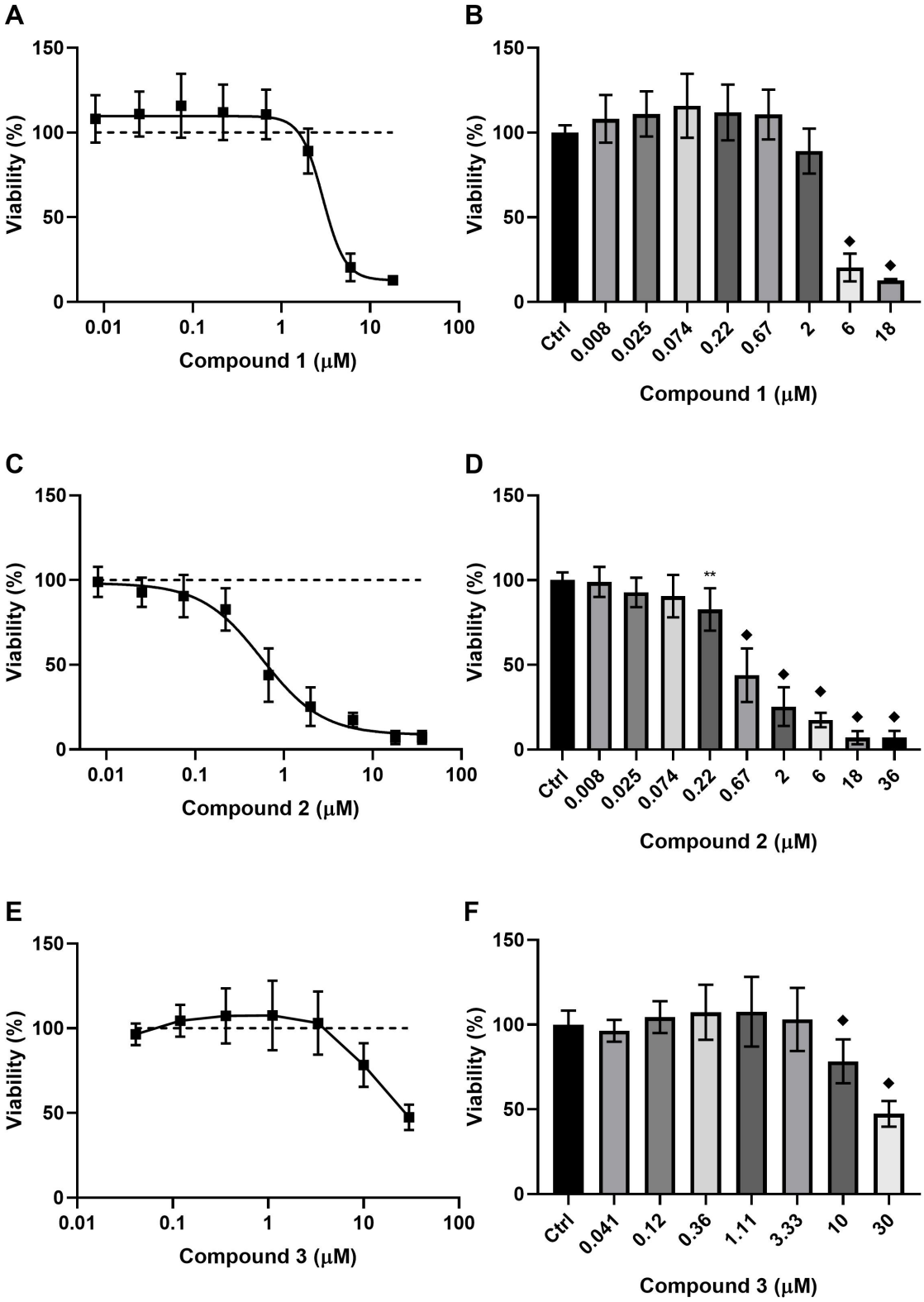
A
Viability (%)
150
100
50
0
0.01
0.1
1
10
100
Compound 1 (μM)
B
Viability (%)
150
100
50
0
Ctrl
0.008
0.025
0.074
0.22
0.67
2
6
18
Compound 1 (μM)
C
Viability (%)
150
100
50
0
0.01
0.1
1
10
100
Compound 2 (μM)
D
Viability (%)
150
100
50
0
**
Ctrl
0.008
0.025
0.074
0.22
0.67
2
6
18
36
Compound 2 (μM)
E
Viability (%)
150
100
50
0
0.01
0.1
1
10
100
Compound 3 (μM)
F
Viability (%)
150
100
50
0
Ctrl
0.041
0.12
0.36
1.11
3.33
10
30
Compound 3 (μM)

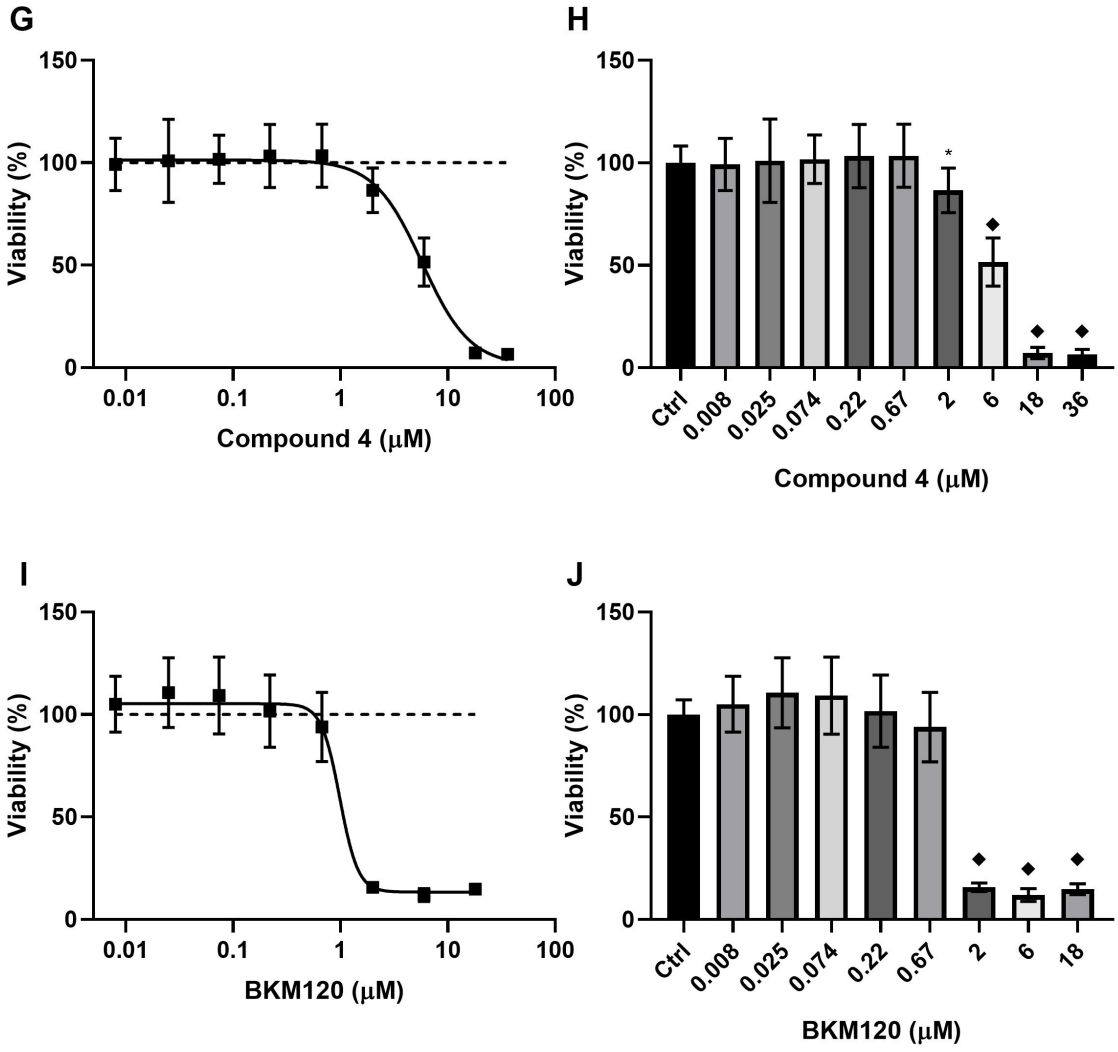

Figure D.6: Dose response correlations of selected cPLA2α inhibitors and BKM120. The dose response curves and bar graphs represent the mean relative viability ± SD across three biological replicates treated for 72 hours in SM. The solid line with black boxes represent the effects of the respective inhibitor, and the dashed line represent the control. Cells treated with 0.0082 - 18 µM of Compound 1 are shown in A and B, 0.0082 - 36 µM of Compound 2 in C and D, 0.041 - 30 µM of Compound 3 in E and F, 0.008 - 36 µM of Compound 4 in G and H and 0.0082 - 18 µM of BKM120 in I and J. Ctrl = Control treatment, set to 100% viability. The dashed line represent the control with 100% viability, and the solid line with black boxes represent the respective inhibitor. * = $p < 0.05$, ** = $p < 0.01$, *** = $p < 0.001$, ◆ = $p < 0.0001$.

Appendix E Additional data - combination assay

Table E.1: Treatments and associated effects given in percent inhibition and combination index (CI) where relevant.

BKM120 (µM)	Compound 1 (µM)	Effect (%)	CI
0.5	-	6.8 ± 7.4	-
0.6	-	8.8 ± 5.3	-
-	2.2	15.2 ± 7.1	-
-	2.4	18.4 ± 8.7	-
-	2.6	31.9 ± 11.9	-
-	2.8	38.0 ± 12.1	-
0.5	2.2	22.7 ± 10.4	0.91
0.5	2.4	28.2 ± 8.1	0.85
0.5	2.6	39.8 ± 7.2	0.92

Table E.2: Treatments and associated effect given in percent inhibition and combination index where relevant.

BKM120 (µM)	Compound 1 (µM)	Effect (%)	CI
0.6	-	15.1 ± 7.3	-
0.7	-	11.3 ± 12.0	-
-	2.0	11.6 ± 10.3	-
-	2.2	19.7 ± 10.0	-
-	2.4	23.1 ± 10.8	-
-	2.6	27.0 ± 13.8	-
0.6	2.0	30.8 ± 7.8	0.81
0.6	2.2	33.8 ± 9.9	0.94
0.6	2.4	42.3 ± 7.1	0.82

Table E.3: Treatments and associated effect given in percent inhibition and combination index (CI) where relevant.

BKM120 (µM)	Compound 2 (µM)	Effect (%)	CI
0.5	-	9.1 ± 5.7	-
0.6	-	9.0 ± 5.5	-
-	0.16	8.3 ± 5.8	-
-	0.20	12.9 ± 9.5	-
-	0.24	15.9 ± 7.1	-
-	0.28	21.8 ± 6.6	-
0.5	0.16	21.8 ± 6.8	0.74
0.5	0.20	26.4 ± 4.9	0.80
0.5	0.24	37.5 ± 7.2	0.62

Table E.4: Treatments and associated effect given in percent inhibition and combination index (CI) where relevant.

BKM120 (µM)	Compound 2 (µM)	Effect (%)	CI
0.6	-	10.3 ± 9.2	-
0.7	-	9.9 ± 9.1	-
-	0.12	8.3 ± 11.4	-
-	0.16	7.6 ± 7.8	-
-	0.20	10.6 ± 12.5	-
-	0.24	24.0 ± 12.4	-
0.6	0.12	21.7 ± 11.1	0.78
0.6	0.16	22.7 ± 13.1	0.75
0.6	0.20	30.3 ± 9.4	0.66

Kristin Lode

Investigating the effects of inhibiting cytosolic phospholipase A2 alpha in an acute lymphoid leukaemia cell model

NTNU
Kunnskap for en bedre verden